openAMUNDSEN v1.0: an open source snow-hydrological model for mountain regions

Ulrich Strasser[1], Michael Warscher[1], Erwin Rottler[1] and Florian Hanzer[1,2]

[1] Department of Geography, University of Innsbruck, Innrain 52, 6020 Innsbruck, Austria
[2] lumiosys GmbH, Innrain 52, 6020 Innsbruck, Austria

Correspondence: Ulrich Strasser (ulrich.strasser@uibk.ac.at)

Abstract. openAMUNDSEN (= the open source version of the **A**lpine **MU**ltiscale **N**umerical **D**istributed **S**imulation **EN**gine) is a fully distributed snow-hydrological model, designed primarily for calculating the seasonal evolution of a snow cover and melt rates in mountain regions. It resolves the mass and energy balance of snow covered surfaces and layers of the snowpack, thereby including the most important processes that are relevant in complex mountain topography. The potential model applications are very versatile; typically, it is applied in areas ranging from the point scale to the regional scale (i.e., up to some thousands of square kilometers), using a spatial resolution of 10–1000 m and a temporal resolution of 1–3 h, or daily. Temporal horizons may vary between single events and climate change scenarios. The openAMUNDSEN model has been applied for many applications already which are referenced herein. It features a spatial interpolation of meteorological observations, several layers of snow with different density and liquid water content, wind-induced lateral redistribution, snow-canopy interaction, glacier ice response to climate, and more. The model can be configured according to each specific application case. A basic consideration for its development was to include a variety of process descriptions of different complexity to set up individual model runs which best match a compromise between physical detail, transferability, simplicity as well as computational performance for a certain region in the European Alps, typically a (preferably gauged) hydrological catchment. The Python model code and example data are available as open source project on GitHub (https://github.com/openamundsen/openamundsen; last access: June 1, 2024).

Copyright statement. TEXT

1 Introduction

The seasonal evolution of the mountain snow cover has a significant impact on the water regime, the microclimate and the ecology of mountain catchments and the downstream river regions (Viviroli et al., 2020; Mott et al., 2023). Snow dominated regions are hence crucial for their inhabitants with their function of collecting, storing, and releasing water resources: more than one sixth of the earth's population relies on seasonal snowpacks (and glaciers) for their water supply (Barnett et al., 2005).

The quantification and prediction of snowmelt amount and dynamics is a challenging task since the complex processes of accumulation, re-distribution and ablation of snow lead to a high variability of the water amount distribution in the mountain snow cover, both in space and time (Viviroli et al., 2007). This high variability challenges both the measuring and modelling of the height and of the water amount of snow (Vionnet et al., 2022), but the understanding of the consequences of climate change on the hydrological effects of a changing mountain snow cover requires an accurate representation of all related processes (Hanzer et al., 2018). Relevant expected changes imply all kind of consequences in the water supply for public and private sectors including hydropower generation, agriculture, forestry and domestic use. Snow processes thereby operate on a variety of spatial and temporal scales (Blöschl, 1999). Further challenges for the modelling of snow processes in mountain regions are imposed by the presence of a forest canopy (Essery et al., 2009; Rutter et al., 2009) which is expected to adapt to the changing climatic conditions and, hence, alter its hydrological effects on the melt rates and the runoff regime from forested mountain regions (Strasser et al., 2011). Finally, the mountain snow cover is an important seasonal landscape feature for all kind of winter touristic activities (Hanzer et al., 2020).

Several types of models with various complexity have been developed to predict the accumulation and ablation of the mountain snow cover (for an overview see Mott et al., 2023). Conceptual models mostly rely on temperature as a proxy for melt rates; their parameters are usually fitted to given streamflow observations (Seibert and Bergström, 2022). Such calibrated temperature index models can provide quite accurate results, since temperature is a physically meaningful replacement of the important energy sources at the snow surface (Ohmura, 2001).

51 Furthermore, temperature is a mostly available observation and comparably handy to be interpolated between local
52 recordings. This type of model has been extended with further elements contributing to the energy balance of the
53 snow surface in various form. E.g., Pellicciotti et al. (2005) included potential solar radiation and parameterized
54 albedo of the snow surface into the modelling, allowing for sub-daily time steps of the calculations.

55 The most sophisticated type of snow model solves the energy balance of the snow surface, requiring a more or
56 less complex description of the short- and longwave radiative fluxes, the turbulent fluxes of sensible and latent
57 heat, the advective heat flux supplied by solid or liquid precipitation and the soil heat flux at the lower boundary
58 of the snow pack. To solve the energy balance equation, these models divide the snowpack into several layers and
59 iteratively compute the state variables for each single layer, usually including respective snow height, density,
60 liquid water content and temperature (e.g., Vionnet et al., 2012; Lehning et al., 1999; Essery, 2015). Sophisticated
61 model concepts of this type also include methods for the correction of the effect of atmospheric stability on the
62 turbulent fluxes (e.g., Sauter et al., 2020).

63 For distributed snow model applications in complex mountain terrain, shadowing of the solar radiation beam and
64 – depending on the application and the considered scale – lateral snow redistribution processes like blowing snow
65 or snow slides should be considered in the modeling, especially if simulations are conducted for longer time
66 horizons (e.g., Vionnet et al., 2021; Quéno et al., 2023). Distributed model applications also require sophisticated
67 methods for the spatial interpolation of the local meteorological station recordings (see, e.g., MeteoIO; Bavay and
68 Egger, 2014), or downscaling procedures to utilize gridded weather or climate model output to force the
69 simulations.

70 Very recently, methods of artificial intelligence have undergone a hype-like push for development of new
71 modelling approaches: these make use of the forcing variables governing any processes changing a system, and
72 time series of observations of its state. In a certain perspective these models are similar to calibrated models, with
73 empirism thereby replaced by statistics. However, the same limitations exist for such statistical approaches like
74 for the empirical ones in terms of transferability of their application in space and time. First attempts also exist to
75 complement complex physical snow models with data-driven machine learning approaches, e.g. the "Deep
76 Learning national scale 1 km resolution snow water equivalent (SWE) prediction model"
77 (https://github.com/whitelightning450/SWEML; last access: June 1, 2024). Similar developments are undertaken
78 in the field of weather forecasting (e.g., Lam et al., 2023), with respective implications on the predictability of the
79 snow cover evolution. It can be expected that in this domain many innovations will emerge in the near future.

80 Most of the sophisticated energy balance snow (hydrological) models which are currently in development are
81 available as open source projects, e.g. Surfex (https://www.umr-cnrm.fr/surfex; last access: June 1, 2024), CRHM
82 (https://github.com/CentreForHydrology/CRHM; last access: June 1, 2024), FSM
83 (https://github.com/RichardEssery/FSM; last access: June 1, 2024), SNOWPACK (https://snowpack.slf.ch; last
84 access: June 1, 2024), COSIPY (https://github.com/cryotools/cosipy; last access: June 1, 2024), or, as described
85 in the following, openAMUNDSEN (https://github.com/openamundsen/openamundsen; last access: June 1, 2024).

86 openAMUNDSEN v1.0, the snow-hydrological model described herein, compromises many of the presented snow
87 model principles, from simple empirical approaches to coupled energy and mass balance calculations. The model
88 mainly is built upon a comprehensive, physically based description of snow processes typical for high mountain
89 regions. In particular, the main features of the model include:

90 • Spatial interpolation of scattered meteorological point measurements considering elevation using a combined
91   regression/inverse distance weighting (IDW) procedure
92 • Calculation of solar radiation taking into account terrain slope and orientation, hillshading and atmospheric
93   transmission losses as well as gains due to scattering, absorption, and multiple reflections between the snow
94   surface and clouds
95 • Adjustment of precipitation using several correction functions for wind-induced undercatch and lateral
96   redistribution of snow using terrain-based parameterizations
97 • Simulation of the snow and ice mass and energy balance using either a multi-layer scheme or a bulk scheme
98   using four separate layers for new snow, old snow, firn and ice
99 • Alternatively, a temperature index/enhanced temperature index method, the latter considering potential solar
100   radiation and albedo of the surface
101 • Usage of arbitrary timesteps (e.g. 10 minutes, hourly or daily) while resampling of forcing data to the desired
102   temporal resolution
103 • Flexible output of time series including arbitrary model variables for selected point locations in NetCDF or
104   CSV format

105 • Flexible output of gridded model variables, either for specific dates or periodically (e.g. daily or monthly),
106 optionally aggregated to averages or totals in NetCDF, GeoTIFF or ASCII grid format
107 • Built-in generation of future meteorological data time series as model forcing with a given trend using a
108 bootstrapping algorithm for the available historical time series of the meteorological recordings
109 • Live view window for the visualization of selectable variables of the model state during runtime.

110 Together with the model, a comprehensive set of data that can be used to run the model for the upper Rofental
111 (Ötztal Alps/Austria, 98.1 km^2) is available at Pangaea (https://doi.org/10.1594/PANGAEA.876120; last access:
112 June 1, 2024) (Strasser et al., 2018) and at https://doi.org/10.5880/fidgeo.2023.037 (last access: July 21, 2024).
113 Further, an openAMUNDSEN example setup is available at GitHub
114 (https://github.com/openamundsen/openamundsen-examples; last access: June 1, 2024). This data can be used to
115 setup and run the model for this catchment and to conduct a multitude of simulation experiments like sensitivity
116 tests and evaluation; it can also serve as example to be replaced by data from other catchments or sites. The
117 Rofental is used also in the following as demonstration site to illustrate the functionalities of the model.

118 2 Model evolution

119 The AMUNDSEN model has a development history of well over twenty years. Originally, the model was prepared
120 to compute fields of meteorological variables, snow albedo and melt with a new enhanced temperature index
121 approach (Pellicciotti et al., 2005). Later, a simple surface energy balance method based on ESCIMO[1] (Strasser
122 and Mauser, 2001) was integrated. The model was then applied and continuously improved to simulate snow
123 hydrological variables for Haut Glacier d'Arolla (Strasser et al., 2004) and the high alpine region of the
124 Berchtesgaden National Park (Strasser, 2008). Strasser et al. (2008) investigated the sublimation losses of the
125 alpine snow cover from the ground and vegetated surfaces, as well as during blowing snow events. In Strasser et
126 al. (2011), snow-canopy processes were modelled for a chess-board pattern of various forest stands and open areas
127 on an idealized mountain. The simple bulk energy balance core of the model also exists as a spread-sheet based
128 point scale scheme where only hourly meteorological variables have to be pasted in to run the snow simulations
129 for a particular observation site (Strasser and Marke, 2010). This spread-sheet based model was later extended by
130 the snow-canopy interaction processes that were already implemented in AMUNDSEN (Marke et al., 2016). The
131 energy balance approach was continuously further developed, e.g. with an iterative procedure to account for
132 atmospheric stability (after Weber, 2008) or with the introduction of a 4-layer scheme (new snow, old snow, firn,
133 glacier ice; Hanzer et al., 2016). Hanzer et al. (2014) developed a module for the production of technical snow on
134 skiing slopes. Historical and future snow conditions for Austria were determined with the model by Marke et al.
135 (2015) and Marke et al. (2018), respectively. Hanzer et al. (2016) presented a parameterization for lateral snow
136 redistribution based on topographic openness, and multi-level spatiotemporal validation as a systematic,
137 independent, complete and redundant validation procedure. The hydrological response and glacier evolution in a
138 changing climate was investigated by Hanzer et al. (2018) for the Ötzal Alps in Austria. Modelled SWE also
139 provided a reference for the fusion with satellite-data derived snow distribution maps in a machine learning
140 framework (De Gregorio et al., 2019a and b), or to determine distributed glacier mass balance (Podsiadło et al.,
141 2020). Pfeiffer et al. (2021) used the model to compute the amount of liquid water provided for infiltration by
142 snowmelt and rainfall for determining conditions that fostered the motion of a landslide in the Tyrolean Alps. With
143 the transition to the open source project openAMUNDSEN, the multi-layer approach by Essery (2015) was
144 integrated into the model as further alternative to compute the mass and energy balance of a layered snow pack.
145 Finally, the openAMUNDSEN model has been used to simulate the entire process of snow management and snow
146 conditions for the slopes in skiing areas (Hanzer et al., 2020, Ebner et al., 2021).

147 The first distributed version of the AMUNDSEN model was developed in IDL (= Interactive Data Language, see
148 https://www.nv5geospatialsoftware.com/Products/IDL; last access: June 1, 2024), originally documented in
149 Strasser (2008) and – in a more recent evolutionary stage – in Hanzer et al. (2018). Recently, the model code was
150 completely re-programmed in Python and transferred into an open source project
151 (https://github.com/openamundsen/openamundsen; last access: June 1, 2024); this was the moment when the
152 model was renamed to "openAMUNDSEN". An online documentation is currently in production
153 (https://doc.openamundsen.org; last access: June 1, 2024). New developments which are not yet available online
154 in the GitHub repository will be published there after comprehensive testing.

---

[1] The first point-scale version of the snow model was named **E**nergy balance **S**now **C**over **I**ntegrated **MO**del
("ESCIMO") and programmed in Fortran (Strasser and Mauser, 2001). Later, when the first distributed version
was developed in IDL, it was renamed to "AMUNDSEN" (Strasser et al., 2004).

3 Model concept

3.1 General structural design

The fundamental principles and most important capabilites of the model are shown in the general overview (figure 1a). The region for which openAMUNDSEN is to be set up is a rectangle comprised by a digital elevation model (DEM) in raster format. This DEM defines the extent and resolution for which the model computations are performed. The model is capable of simulating the mass balance of both snow and/or glacier ice surfaces, as well as lateral redistribution of snow, snow-canopy interaction and evapotranspiration from different land cover types. Irregular observations of meteorological stations or gridded output from any kind of raster model are distributed over the domain by means of an IDW procedure considering dependence on elevation in each timestep and spatially interpolated local residuals of the recordings (figure 1b); alternatively, fixed monthly gradients can be applied. Several approaches of vaying complexity are available to compute surface melt, from a simple temperature-index method over an enhanced index approach considering temperature, potential solar radiation and albedo to sophisticated energy balance methods (figure 1c). These melt approaches can be combined with two layering schemes in a total of four different snow model configurations. Each of these configurations can be applied to forest conditions, where a modified set of the meteorological variables is provided to account for the effect of the trees on the inside-canopy microclimatic conditions, parameterized by means of the Leaf Area Index (LAI) as the variable describing the characteristics of the forest (figure 1d).
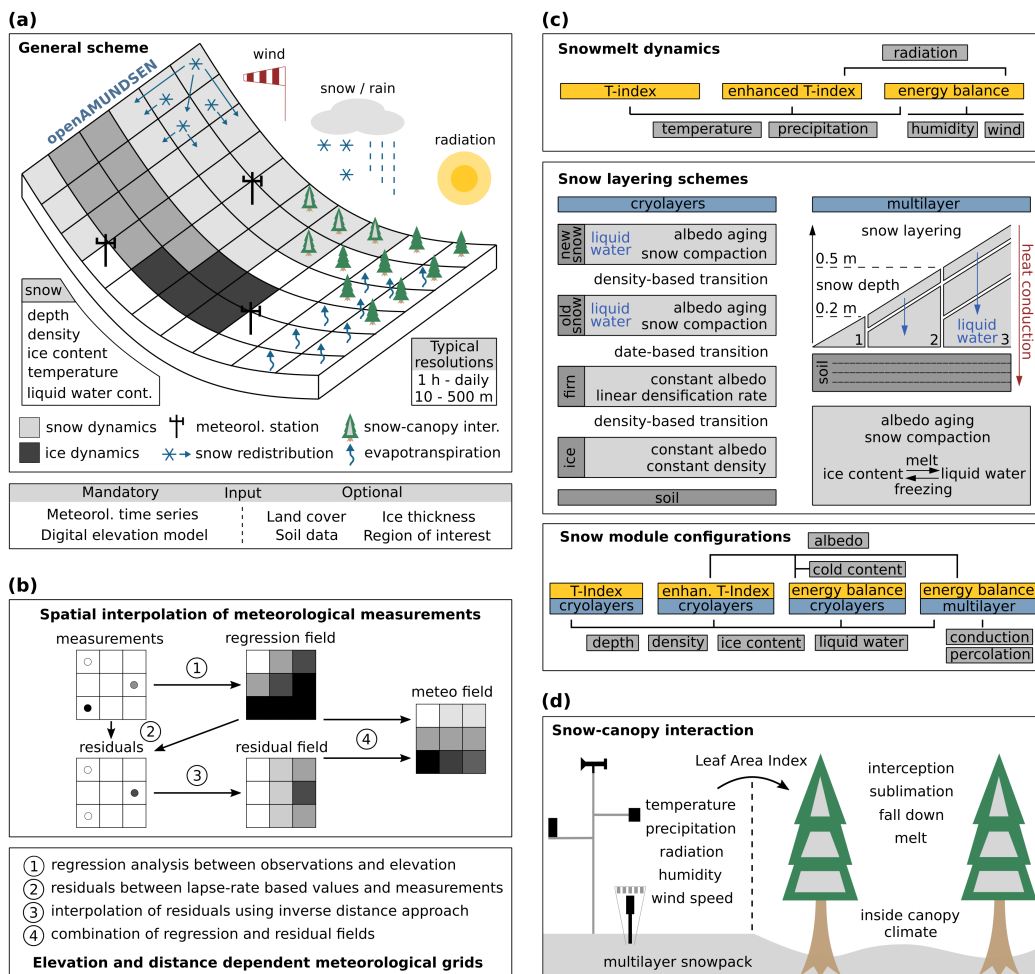

Figure 1: Schematic representation of a domain modelled with the snow-hydrological model openAMUNDSEN (a), spatial interpolation of the meteorological measurements (b), snowmelt dynamics and snow layering schemes and (c) and scaling of observed to inside-canopy meteorological conditions for the simulation of snow-canopy interaction processes (d) in the model.

To save computational time, it is possible to define an irregular region of interest (ROI; i.e., a sub-quantity of pixels); outside this area only some calculations required for the interpolation of the meteorological variables will be computed (figure 2a). Typically, a ROI is a watershed area for which water balance components are aggregated

180   from the single pixel values so that resulting streamflow volume can be compared to gauge recordings (Hanzer et
181   al., 2018). Weather stations to be considered can also be located outside the ROI or even outside the DEM area;
182   however, in the latter case they cannot be considered for the determination of shadow areas or regional-scale
183   albedo which is used to estimate the diffuse radiative fluxes by multiple scattering between the surface and the
184   atmosphere. Extent and resolution of the DEM defines the cell size and the geometry of all other raster layers
185   produced in the simulations (figure 2b). From this DEM, several derived variables such as slope, aspect and sky
186   view factor are calculated (figure 2c). The sky view factor is the ratio of the visible sky that can be seen from a
187   pixel location to the entire hemisphere that contains both visible and obstructed sky.
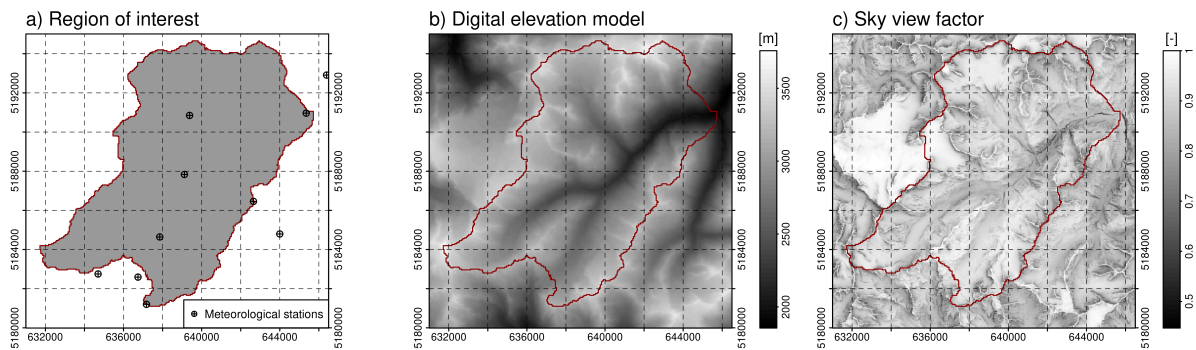
189   Figure 2: Region of interest (ROI) of the openAMUNDSEN example application to the Rofental (Ötztal
190   Alps/Austria) with location of weather stations in- and outside this region of interest (a), digital elevation model
191   (b) and sky view factor (c). The red line is the watershed divide of the Rofental for the gauge at Vent (1891 m
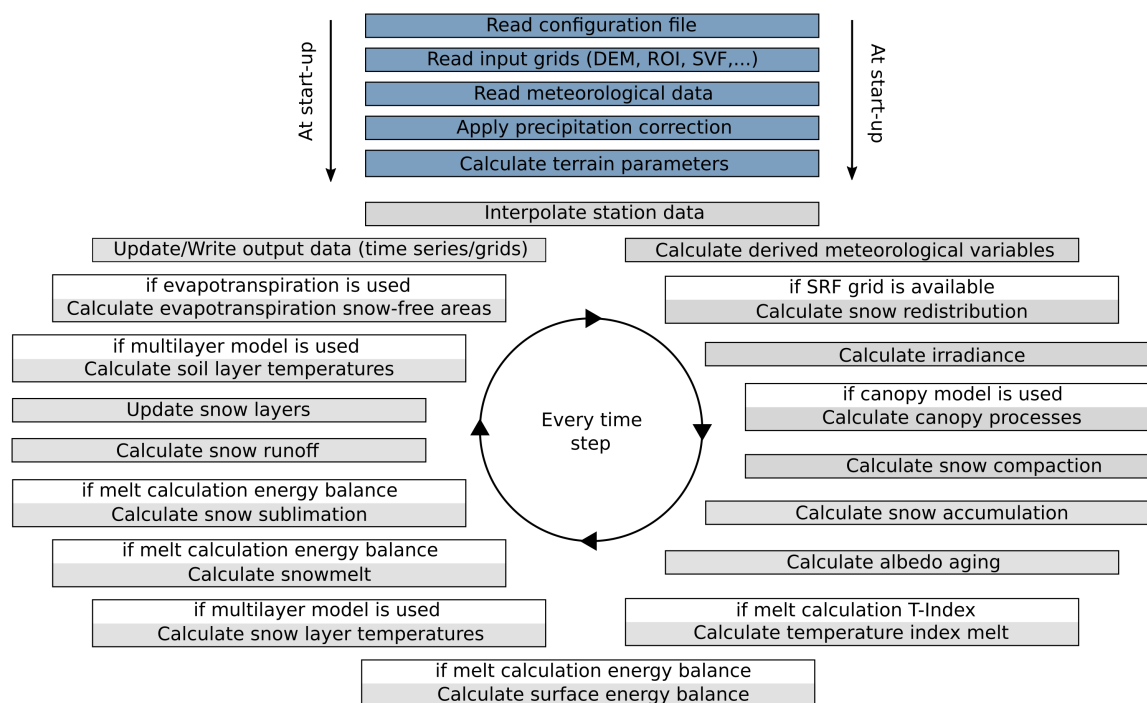192   a.s.l.).

193   The meteorological forcing for the simulations typically consists of time series of temperature, relative humidity,
194   precipitation, global radiation and wind speed. These variables are standard observations at the meteorological
195   stations of operational weather services and mostly available for many mountain regions (e.g. in Austria:
196   www.geosphere.at; last access: June 1, 2024). To accurately track the daily course of radiative energy – usually
197   the most important component of the energy for melt (Strasser et al., 2004) – the time step in the modelling in
198   most applications is hourly. To save computational time, the model computations can also be limited to 2- or 3-
199   hourly time steps. If the optional temperature index approach is selected the time step also can be set to daily. For
200   the case that specific submodules are activated for a model run (e.g., snow-canopy interaction or
201   evapotranspiration), various other spatial input fields have to be prescribed (e.g., land cover, soil and/or catchment
202   boundaries).

203   When using meteorological station data as input the minimum number of stations required is one. This station
204   should provide a continuous series of measurements without gaps. If more than one weather station exists, missing
205   values at a particular site are replaced by the respective results from the interpolation procedure. Where recordings
206   exist, the interpolated values might slightly differ due to the difference in altitude between the exact location of
207   the station and the grid pixel in which it is located (and for which the meteorological field is interpolated).
208   Alternatively to station recordings, it is also possible to provide pre-processed gridded meteorological fields as
209   input to the model, e.g. output data from numerical weather prediction or climate models. Data timeseries of future
210   climate evolution to force openAMUNDSEN for climate change scenario simulations can be produced by means
211   of a stochastic block bootstrap resampler which is realized as external routine in Python (see Appendix).

212   The model simulations are performed for each pixel and each timestep (figure 3). Prior to these pixel-wise
213   computations for the raster domain a set of general computations for the model run are performed: after reading
214   the input data the terrain parameters are computed from the DEM, and precipitation correction parameters are
215   computed (as described in 3.5). Then the time-dependent computations for all pixels of the domain start, in a loop
216   from the first to the last time step of the particular simulation run. Several modules are subject to options which
217   can be set in a configuration file in text format.

218   The results of the computations can be written to file either as time series for an arbitrary number of pixels (in
219   NetCDF or CSV format), or as gridded model variables for specific selected dates or periodically (e.g., daily,
220   monthly or yearly), optionally aggregated to averages or totals. Possible formats include NetCDF, GeoTIFF and
221   ASCII grid.

222 To keep modelling time to a minimum, state variables (e.g., from a spin-up simulation) can be imported as raster
223 grids to initialize an openAMUNDSEN model run. Some state variables can also be computed prior to the model
224 run. E.g., if glacier outlines are available, the initial ice thickness distribution can be calculated using the approach
225 by Huss and Farinotti (2012). Volumetric balance fluxes of individual glaciers can be calculated from mass balance
226 gradients and constants. Surface elevations and glacier outlines are usually published in glacier inventories
227 (https://wgms.ch/; last access: June 1, 2024), e.g. for Austria in Fischer et al. (2015).

228

At start-up

Read configuration file
Read input grids (DEM, ROI, SVF,...)
Read meteorological data
Apply precipitation correction
Calculate terrain parameters

At start-up

Interpolate station data

Update/Write output data (time series/grids) — Calculate derived meteorological variables

if evapotranspiration is used
Calculate evapotranspiration snow-free areas

if SRF grid is available
Calculate snow redistribution

if multilayer model is used
Calculate soil layer temperatures

Calculate irradiance

Update snow layers

if canopy model is used
Calculate canopy processes

Calculate snow runoff

Calculate snow compaction

if melt calculation energy balance
Calculate snow sublimation

Calculate snow accumulation

if melt calculation energy balance
Calculate snowmelt

Calculate albedo aging

if multilayer model is used
Calculate snow layer temperatures

if melt calculation T-Index
Calculate temperature index melt

Every time step

if melt calculation energy balance
Calculate surface energy balance

229 Figure 3: Flowchart showing the repetetive circle of a typical openAMUNDSEN model run. The reading of the
230 input is succeeded by the computation of several precipitation correction and terrain parameters. After that, the
231 loop for all time steps of the model run is entered.

232 3.2 Temporal and spatial discretization

233 Usually the model is driven with a temporal resolution according to the one of the used meteorological forcing
234 variables. For model applications which require a higher temporal resolution (or if only daily recordings are
235 available) methods exist to disaggregate the measurements accordingly (e.g. MELODIST; Förster et al., 2016).
236 For simulations with lower temporal resolution than the forcing, aggregation is done during runtime. Output
237 temporal resolution can be any aggregate of the original computation resolution – usually daily, monthly and
238 yearly. All this is arbitrarily set in the model configuration prior to the model run. The minimum spatial resolution
239 is not limited. Theoretically, a 1 m or even higher resolution (e.g. laser-scan derived) DEM can be used as basis
240 for the model simulation. A comparatively high resolution thereby is beneficial for adequately capturing all small-
241 scale processes shaping the snow cover distribution in complex terrain. However, it is questionable if such
242 computational effort is meaningful with respect to the availability and quality of the forcing data and to the scale
243 of the considered processes. According to our experiences from typical mountain catchments in the European
244 Alps, a resolution between 10 m and 1000 m is often a good compromise between detail representation and
245 computational efficiency. The size of the modelled domain can be anything between one single pixel and some
246 thousands of square kilometers (see figure 1a). De Gregorio et al. (2019a, b), e.g., successfully applied the model
247 for the Euregio Tyrol/South Tyrol/Trentino (Austria/Italy) which has a size of 26254 km^2.

248 3.3 Spatial interpolation of meteorological measurements

249 openAMUNDSEN includes a meteorological pre-processor for the spatial interpolation of scattered point
250 measurements, irrespective whether these are provided irregularly (weather station recordings) or arranged as a
251 regular grid (raster stack of weather or climate model output). In the latter case, the meteorological variables are
252 resampled to grids with the given DEM spatial resolution. The minimum forcing required by the model consists
253 of recordings of temperature and precipitation (when running in temperature index mode). For energy balance
254 calculations, relative humidity, global radiation (or cloudiness) and wind speed are required in addition. If

255 meteorological time series from station recordings are used as input, the model interpolates the measurements
256 from their geographical locations to each grid cell inside the ROI (figure 4). In most simulation cases, recordings
257 of the meteorological variables for the 2 m observation level are available. The distance between a variable snow
258 surface and the sensor height can therefore be corrected in the modelling. To spatially interpolate the station
259 observations in each model time step, the following IDW-based interpolation procedure is applied:

260 • a regression analysis between observations and the associated station elevation is performed to derive an
261 elevation-dependent trend function: the lapse rate (LR)
262 • the derived function is applied to all cells of the DEM to create an elevation trend field for each meteorological
263 variable, the "regression field" (figures 4a and 4d)
264 • the residuals for all station locations are calculated by subtracting the calculated regression value for the
265 station elevation from the actual measurement at the station location for the current time step,
266 • the residuals for the station locations are interpolated to the grid using an IDW method, resulting in the
267 "residual field" (figures 4b and 4e),
268 • this interpolated residual field is added to the regression field, which results in elevation- and station distance-
269 dependent interpolated fields for all meteorological variables (figures 4c and 4f).

270 Figure 4 exemplarily shows the steps of this IDW-based interpolation procedure for temperature and precipitation.
271 It can be seen that for both meteorological variables a dependency of the recordings with elevation does exist
272 (figure 4a and 4d), but locally some deviations of the measurements from the elevation trend occur (figure 4b and
273 4e). In the result both patterns are visible. The procedure automatically fills potential gaps in the observation time
274 series at the weather station locations. If only one observation for the LR determination exists at a given time step
275 for the entire domain this one observed value is uniformly distributed over the domain.
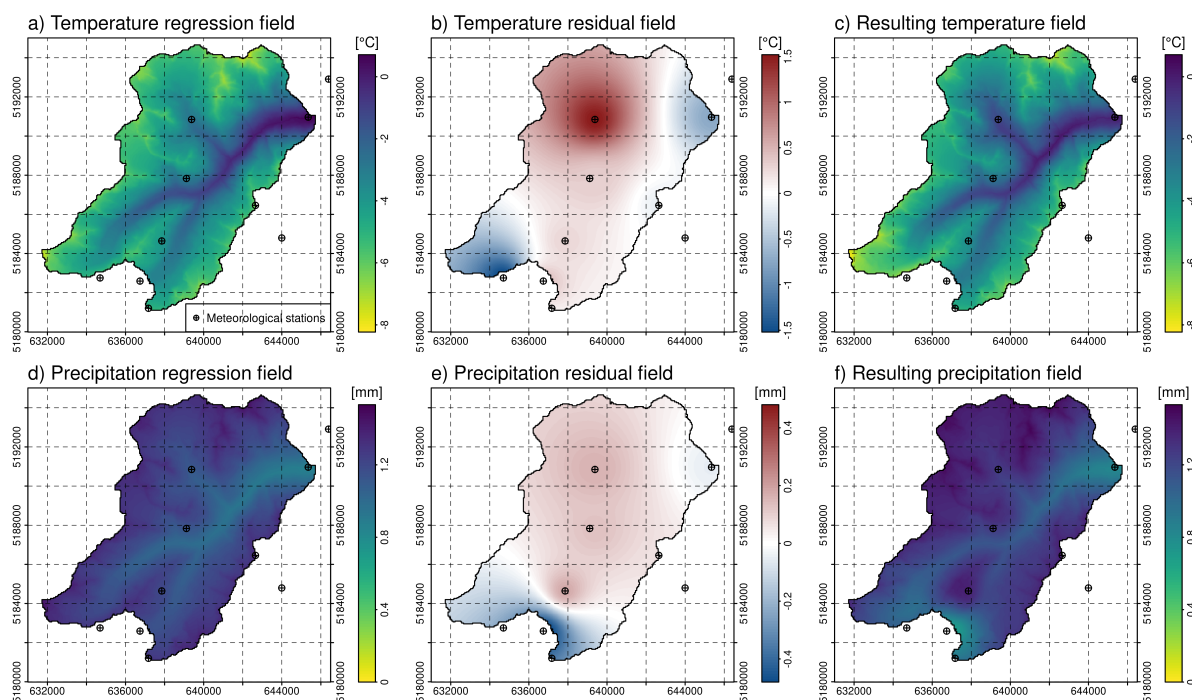
276

277 Figure 4: Regression field, residual field and the resulting meteorological field, i.e. sum of the two for the spatial
278 interpolation of meteorological variables in each single time step, exemplarily shown for temperature (a, b and c)
279 and for precipitation (d, e and f) on 24/12/2019 at 10 am for the Rofental. The resolution of the interpolated grid
280 is 20 m.

281 Instead of the dynamic LR calculated from the local observations in each time step, the prescribed average monthly
282 values of MicroMet (Liston and Elder, 2006) can be used. MicroMet is a quasi-physically based meteorological
283 observation distribution system of intermediate complexity to produce high-resolution atmospheric forcings
284 required to run spatially distributed terrestrial models in complex topography. It distributes the variables air
285 temperature, relative humidity, wind speed, incoming solar (shortwave) and longwave radiation, surface pressure
286 and precipitation following a Barnes objective analysis scheme, similar to the IDW procedure applied in
287 openAMUNDSEN. A detailed comparison of results achieved with the interpolation schemes of

288 openAMUNDSEN, MicroMet (and others, e.g. MeteoIO; Bavay and Egger, 2014) and respective effects on the
289 snow processes modelling would be an interesting task of scientific value, but is beyond the scope of this paper.
290 Here we only demonstrate the dynamic (mostly hourly) derived from the station observations in
291 openAMUNDSEN for the Rofental and their monthly averages compared to the standard temperature LR and
292 monthly values originating from other regional contexts (figure 5): e.g., the monthly average temperature LR
293 derived for the Upper Danube catchment in central Europe are several degrees above the ones derived for the
294 Northern Hemisphere; this shows the necessity of calculating LR using local observations. It should be noted,
295 however, that dynamic temperature LR and their monthly averages may vary from year to year.
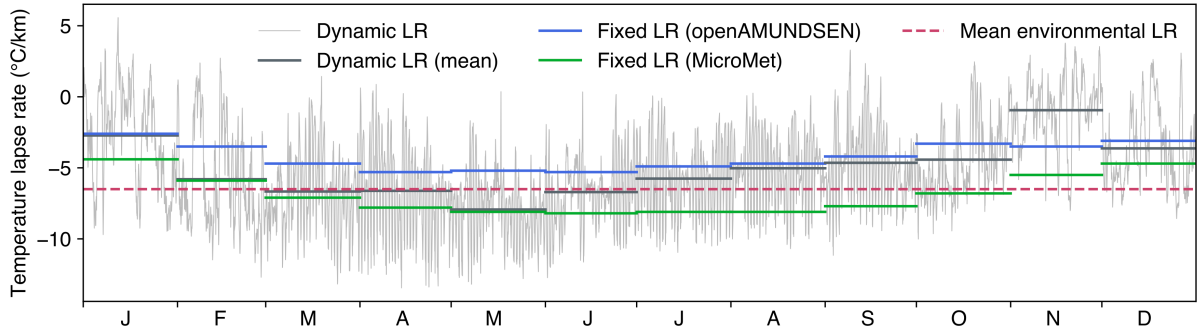
296

297 Figure 5: Dynamic (mostly hourly) temperature LR for 2020 in the Rofental (gray). The fixed LR are monthly
298 averages derived for the Upper Danube catchment (blue; Marke, 2008) and the Northern Hemisphere (green;
299 Liston and Elder, 2006). The dashed line shows the mean environmental LR of –6.5 °C km^{-1}. Monthly averages
300 computed for the dynamic LR (derived from the observations in each model time step) are dark grey.

301 Finally, precipitation phase is determined in openAMUNDSEN by either air temperature or wet-bulb temperature
302 thresholds (wet-bulb temperature is computed by iteratively solving the psychrometric equation). For both
303 methods, a temperature transition range is defined. Above this transition range, precipitation is determined as
304 liquid, and as solid below the lower end of the temperature range, respectively. Within the defined temperature
305 range, the fractions of solid/liquid precipitation are linearly distributed between 100 % liquid at the upper and 100
306 % solid at the lower end of the range with 50 % liquid/solid fraction of precipitation at the threshold temperature.
307 The threshold used in the presented simulations here was chosen empirically: a value of 0.5 °C wet bulb
308 temperature with a transition extent from 0 °C to 1 °C produced reliable results in many numerical experiments
309 with the model, in particular for the well-gauged site Rofental (see Hanzer et al., 2016).

310 3.4 Radiative fluxes

311 Incoming global radiation strongly varies in time and space depending on terrain characteristics, position of the
312 sun and atmospheric conditions. Hence, openAMUNDSEN calculates potential global radiation for each grid cell
313 based on local aspect and slope, position of the sun, orographic shadows, atmospheric transmission losses and
314 gains due to scattering, absorption and reflections, multiple reflections between snow and clouds as well as
315 reflected radiation from snow covered neighbouring slopes. Cloud coverage (when not prescribed) is either
316 determined by comparing potential to observed global radiation; or, alternatively, it is estimated using atmospheric
317 humidity following Liston and Elder (2006). During nighttime either the atmospheric humidity approach is used
318 or cloudiness is kept constant. In the final step, cloud coverage is spatially interpolated and actual incoming global
319 radiation is calculated by correcting potential global radiation with cloud coverage for each model grid cell.

320 Reflected short wave radiation depends on surface albedo which strongly varies in space and time, for snow
321 surfaces mainly depending on grain size. In openAMUNDSEN, albedo is modelled taking into account snow age
322 and an air temperature-dependent decay function following Rohrer (1992) and Essery et al. (2013):

323
$$\alpha = \alpha_{min} + (\alpha_{t-1} - \alpha_{min}) \cdot e^{-\frac{1}{\tau}\delta t}$$

324 where α_{min} is the (prescribed) minimum albedo, α_{t-1} the albedo in the previous time step, δt the time step length,
325 and τ is a temperature-dependent recession factor (implemented by prescribing two factors τ_{pos} and τ_{neg} for positive
326 and negative air or, optionally, surface temperatures). Maximum snow albedo α_{max} is by default set to 0.85, while
327 α_{min}, τ_{pos}, and τ_{neg} are set to 0.55, 200 h, and 480 h. Firn and ice albedo are held constant with $\alpha_{firn} = 0.4$ and $\alpha_{ice} =$
328 0.2 by default. Fresh snow increases albedo, either using a step function – increasing albedo to α_{max} when a

329 snowfall above a certain threshold amount per timestep (default: 0.5 kg m^{-2} h^{-1}) occurs – or using the continuous
330 function

$$\alpha = \alpha_{t-1} + (\alpha_{max} - \alpha_{t-1})\frac{S_f}{S_0},$$

332 where S_f is the snowfall amount and S_0 the snowfall required to refresh albedo (Essery et al., 2013).

333 Incoming longwave radiation from the atmosphere is a function of atmospheric conditions and temperature and is
334 determined using the Stefan-Boltzmann law. Atmospheric emissivity thereby depends on water vapour content in
335 clear sky conditions and cloud cover in overcast situations. Additionally, openAMUNDSEN accounts for long-
336 wave radiation from the neighbouring slopes. Outgoing longwave radiation is calculated following the Stefan-
337 Boltzmann law with the emissivity of snow and modelled snow surface temperature. The details of the radiation
338 model mostly follow Corripio (2002) and are described in Strasser et al. (2004).

339 **3.5 Precipitation correction**

340 Precipitation measurements are vital input for every snow-hydrological model. However, measuring solid
341 precipitation in complex alpine terrain is prone to large errors which typically results in an undercatch of
342 precipitation (Rasmussen et al., 2012). This is particularly important for mountain regions with a high amount of
343 solid precipitation. High wind speeds can cause an undercatch of snowfall up to 50 % (Kochendorfer et al., 2017)
344 when using typical pluviometers of the Hellmann type. For solid precipitation, different correction methods are
345 implemented in the model in order to account for the undercatch of precipitation gauges when measuring snow
346 accumulation. Hanzer et al. (2016) showed that a combination of a weather station-based snow correction factor
347 taking into account wind speed and air temperature based on an approach by the World Meteorological
348 Organization (WMO; Goodison et al., 1998) with a subsequent constant post-interpolation additional factor
349 yielded plausible precipitation amounts. Whereas the first correction is applied for the station recording amount
350 prior to interpolation to the cells of the rectangular grid, the latter is added to all grid cells of the modelling domain.
351 Alternatively to the WMO approach, a method which estimates undercatch regardless of precipitation phase
352 (Kochendorfer et al., 2017) can be selected in the model configuration procedure prior to a model run.

353 **3.6 Snow redistribution**

354 Irrespective whether rain or snow, with the IDW interpolation scheme in openAMUNDSEN the amount of
355 precipitation is distributed over the domain depending on the grid cell elevation, the distance of the surrounding
356 weather stations and the selected gauge undercatch correction method. The amount of observed snow at a certain
357 location, however, can be significantly affected by the lateral processes of preferential deposition, erosion and
358 lateral redistribution. These processes are driven by wind and gravitational forces (Warscher et al., 2013;
359 Grünewald et al., 2014). Many approaches with different complexity exist to account for these processes; a recent
360 and comprehensive overview of modelling lateral snow redistribution is given by Quéno et al. (2023). Such
361 consideration of the lateral snow redistribution processes is required to prevent artefacts of continuous snow
362 accumulation on high summits and crests in long-term simulations where melt during summer is not sufficient to
363 remove the amount of snow accumulated during the previous winter. The result will be that with increasing
364 simulation period, in such locations "snow towers" will continuously grow, whereas in depressions beneath snow
365 accumulation will be underestimated (Freudiger et al., 2017). As a consequence, mass balances of existing glaciers
366 in such locations will be increasingly wrong due to not enough mass deposited in the accumulation areas. Mass
367 balances therefore are a useful measure to evaluate the simulations with respect to the lateral snow redistribution
368 processes, as demonstrated by Hanzer et al. (2016). In openAMUNDSEN a snow redistribution factor (SRF) field
369 can be used to parameterize spatial snow distribution. The SRF describes the fractional amount of snow either
370 eroded or deposited at each pixel location and modifies the interpolated snowfall field accordingly. Since SRF
371 derivation can depend on various topographic parameters such as elevation, slope, aspect, curvature, viewshed or
372 terrain roughness, and generally requires site-specific calibration (Grünewald et al., 2013), openAMUNDSEN
373 allows for flexibility in calculating the SRF field. It provides functions to compute these topographic parameters
374 but does not prescribe a singular method for final SRF calculation. Instead, the user of the model can decide in
375 which way the snow redistribution should be parameterized in the model and if and how the results of the selected
376 method should be calibrated and evaluated.

377 In the presented application for the Rofental, the concept of negative topographic openness (Yokoyama, 2002) has
378 been used to parameterize spatial snow distribution. It is obtained by averaging the nadir angles calculated for all
379 eight compass directions from the grid point, yielding low values for convex topographic features and high values

for concave topographic features. The openness values finally depend on a length scale which describes the spatial dimension of the given topographic features affecting the redistribution processes, resulting in a snow redistribution factor which describes the fractional amount of snow eroded or deposited for any pixel location. The length scale depends on the shape and size of the topographic features of a landscape and the spatial resolution of the used DEM and should therefore be determined for each modelling domain and model application separately. For the example presented here it has been empirically determined for the area of the Ötztal Alps (Austria) by Helfricht (2014). Effectively, the SRF approach as parameterized in openAMUNDSEN takes into account the processes of preferential deposition, wind-induced erosion, saltation and turbulent suspension of atmospheric (snow) precipitation. The way it is implemented in the model, however, does not account for single events of lateral snow redistribution, but for their accumulated effect over longer simulation periods. Figure 6 shows an example of a snow redistribution factor field calculated using a combination of negative openness fields using two different length scales L (Hanzer et al., 2016): negative openness was calculated for the entire Ötztal mountain range based on a 50 m DEM for L = 50 m and L = 5000 m. Whereas the smaller value accounts for small-scale topographic features with a high spatial variability, with the higher value the large-scale topography of ridges and valley floors are considered, and hence the overdeepening of the surface elevation of glacier tongues compared to the surrounding ridges and peaks (Helfricht, 2014). Details of the computation are given in Hanzer et al. (2016). Results show the (red) areas of the summits and ridges where snowfall is significantly reduced, whereas in the slopes and valley bottoms it is subsequently accumulated (blue areas; figure 6a. Correspondingly, in the presented example the respective exposed areas receive much less precipitation in May 2018 than the slopes and downvalley areas (figure 6b).
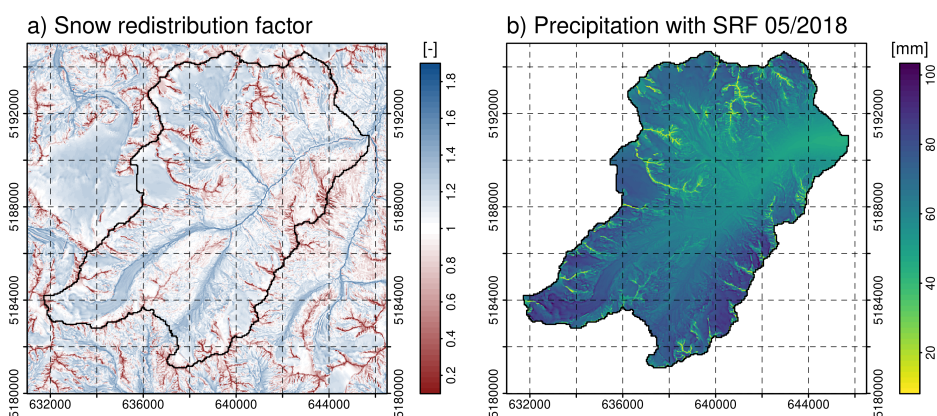
Figure 6: The snow redistribution factor (SRF) used in openAMUNDSEN to compensate for snow erosion on exposed ridges and for snow deposition in the slopes and depressions beneath (a) and an example of monthly total precipitation with lateral redistribution of snowfall (for May 2018), determined with the snow redistribution factor (b).

Together, three snow amount corrections can be applied in openAMUNDSEN: (i) a windspeed and temperature-dependent precipitation correction at the site of the measurement, (ii) an additional post-interpolation factor (see 3.5 for a description of how this is modelled), and (iii) the presented adjustment accounting for lateral snow redistribution. Whereas (i) and (ii) increase the amount of measured precipitation towards a more realistic volume over the entire grid, (iii) solely redistributes the solid amount of precipitation from areas of erosion to areas of deposition.

3.7 Snow-canopy interaction

Forest canopies generally lead to a reduction of global radiation, precipitation and wind speed at the ground, whereas humidity and long-wave radiation are increased and the diurnal temperature cycle is dampened. In openAMUNDSEN, the micrometeorological conditions for the ground beneath a forest canopy are derived from the interpolated measurements (assuming the weather stations are located in the open) by applying a set of modifications for these meteorological variables. The modifications are based on the effective Leaf Area Index of the trees composing the stands, i.e. the sum of the classical LAI and the Cortex Area Index CAI (Strasser et al., 2011). By means of the modified meteorological variables, the processes of interception, sublimation, unloading by melt and fall down by exceeding the canopy snow-holding capacity are calculated. Liquid precipitation is assumed to fall through the canopy and is added to the ground snow cover (see figure 1d).

421 Simulations with the snow-canopy interaction model for an idealized mountain (Strasser et al., 2011) showed that,
422 despite reduced accumulation of snow on the ground beneath the trees, both rates and seasonal totals of sublimation
423 of snow previously intercepted in a canopy were significantly higher than the sublimation losses from the ground
424 snow surface. On top of that, shadowing leads to reduced radiative energy input inside the canopy and hence
425 protection of the snow at the ground. The type of forest, exposition, the specific meteorological conditions and the
426 general evolution of the winter season play important roles as well: during winter, the effect of reduced
427 accumulation is dominant, whereas during spring, the shadowing effect with reduced ablation prevails. In winters
428 with much snow, the effect of shadowing by the trees dominates and snow lasts longer inside the forest than in the
429 open. In winters with little snow, however, the sublimation losses of snow are dominant and the snow lasts longer
430 in open areas. This migh vary, however, for northern and southern exposure to radiation and time of the year due
431 to the strong effect of solar radiation on melt. In early and high winter, the radiation protection effect of shadowing
432 is small. An intermittent melt out of the snow cover beneath the trees can occur if little snow is available. The
433 shadowing effect becomes more efficient and snowmelt is delayed relative to nonforested areas in late winter and
434 spring. Due to the combination of all these processes, the modelling of snow-canopy interaction can lead to
435 complex and very heterogeneous patterns of snow coverage and duration in alpine regions with forest stands
436 (Essery et al., 2009; Rutter et al., 2009; Strasser et al., 2011).

437 3.8 Crop evapotranspiration

438 For non-snow-covered surfaces the actual evapotranspiration of vegetated areas is calculated using the Food and
439 Agriculture Organisation (FAO) Penman-Monteith approach (Allen et al., 1998), for which a schematic overview
440 is illustrated in figure 7. In a first step, the evapotranspiration is calculated for a reference crop (grass) using the
441 meteorological variables and a limiting amount of available water in the soil storage. In forested areas, thereby the
442 inside-forest meteorological conditions are considered. Then, the resulting evapotranspiration is modified
443 according to the vegetation type using particular crop coefficients which integrate the effects of plant height,
444 albedo, stomata resistance and exposed soil fraction. Crop coefficients are available for a wide range of plant types
445 in the given literature and change their values seasonally according to predefined growth stage lengths. For each
446 plant type, evapotranspiration can either be calculated using a single-coefficient approach which integrates the
447 effects of crop transpiration and soil evaporation into a single coefficient, or using a dual-coefficient approach
448 which considers crop transpiration and soil evaporation separately. Soil evaporation is computed considering the
449 cumulative depth of water evaporated from the top soil layer and the fraction of the soil surface that is both exposed
450 and wetted. The soil type thereby determines the amount of evaporable water with respect to field capacity, water
451 content at wilting point and depth of the surface soil layer that is subject to drying by means of evaporation (0.10
452 to 0.15 m); parameters are available for sand, loamy sand, sandy loam, loam, silt loam, silt, silt clay loam silty
453 clay and clay (Allen et al., 1998). With this approach the water balance of the upper soil layer is computed,
454 determining if surface runoff and deep percolation can occur or if evapotranspiration is limited. If the
455 evapotranspiration module is activated, both soil types and land cover must be available as rasterized maps in the
456 DEM geometry.

457
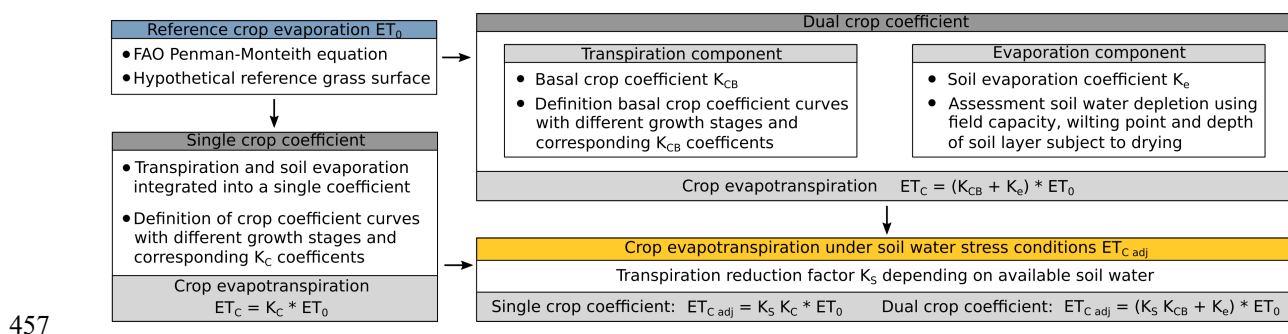
458 Figure 7: Schematic overview of the FAO evapotranspiration module to compute the water flux from the soil
459 throught the plants to the atmosphere with the Penman-Monteith equation. Fluxes are calculated for a reference
460 crop and then scaled to other landuse classes.

461 3.9 Layering schemes

462 In openAMUNDSEN two different layering schemes for snow- or ice-covered surfaces are implemented (see
463 figure 1c). The "cryospheric layer version" parameterizes layers of new snow, old snow, firn and glacier ice. The
464 advantage of using these layers is that they are distinctively different in their optical properties, and hence their

11

465 surfaces can be recognized and distinguished in the field, on photographs, or by satellites with sensors sensitive in
466 the visible range of the electromagnetic spectrum. The model tracks the thickness of these layers and parameterizes
467 their density with more or less empirical relations. For the snow-soil interface a fix upwards heat flux can be set
468 (often 2 W m^{-2} in the Alpine region). The most comprehensive descriptions of this model versions can be found
469 in Strasser (2008), Strasser et al. (2011) and Hanzer et al. (2016).

470 The "multi-layer version" is adopted following the structure of the FSM model (Essery, 2015). It considers a
471 number of layers (by default three) with fixed maximum depths (for the upper two ones), all of them without
472 physical representation. In this model version the fluxes of mass and energy are tracked by means of an iterative
473 computation of the state variables temperature and liquid water content such that the balances of mass and energy
474 are closed for each layer. The energy transfer at the snow-soil interface is calculated by means of a 4-layer soil
475 model. A detailed description of the implemented multi-layer model scheme can be found in Essery (2015).

476 Whereas the cryospheric layer version of openAMUNDSEN can be combined with both the simple or the enhanced
477 temperature-index approach or, alternatively, with the energy balance method, the multi-layer version requires the
478 energy balance method to compute the energy and mass balances of the surface and the snow layers beneath. The
479 simulation of glacier evolution as a response to the climatic conditions presupposes the cryospheric layer version
480 to be applied.

481 3.9.1 Cryospheric layer version

482 In the cryospheric layer version of openAMUNDSEN, the transitions between new snow and old snow occur when
483 reaching a predefined snow density threshold (by default 200 kg m^{-3}), while remaining snow amounts at the end
484 of the ablation season are transferred to the firn layer (by default on 30 September). Compaction for the new and
485 old snow layers is calculated using the methods described below (in 3.10); for firn a linear densification is assumed.
486 Once reaching a threshold density of 900 kg m^{-3}, firn is added to the ice layer beneath. While snow albedo is
487 parameterized using the aging curve approach (Rohrer, 1992), firn and ice albedo is kept constant (with default
488 values of 0.4 and 0.2, respectively). The details of the cryospheric layer version of openAMUNDSEN are best
489 described in Hanzer et al. (2016).

490 While snow temperature of the individual layers is not calculated using the cryospheric layering scheme, an
491 approach following Braun (1984) and Blöschl and Kirnbauer (1991) is applied in order to determine an average
492 cold content of the snow layers. This cold content builds up when the snowpack cools; it has to be depleted before
493 melt and subsequent runoff can occur at the snowpack bottom. The maximum possible cold content is thereby set
494 to 5 % of the total snowpack weight (the latter can be converted to an energy by multiplication with the latent heat
495 of fusion).

496 When using this scheme, the snowpack is taken as a bulk layer to solve the surface energy balance. If air
497 temperature is above 0 °C the model assumes that the snow surface temperature is 0 °C and melt occurs, the
498 amount of which can be computed from the available excess of the energy balance. If the air temperature is below
499 0 °C, an iterative procedure to compute the snow surface temperature for closing the energy balance is applied.
500 With this procedure, the snow surface temperature is altered until the residual energy balance passes zero.

501 3.9.2 Multi-layer version

502 In the multi-layer version of openAMUNDSEN, the vertical heat fluxes are computed through both the snow pack
503 and into the ground (Essery, 2015). To solve the energy balance, melt is first assumed to be zero for the surface
504 temperature change of every timestep. Snow is melting if the energy balance results in a surface temperature
505 passing 0 °C. The temperature increment is recalculated assuming that all of the snow melts; if this results in a
506 surface temperature below 0 °C, snow only partially melts during the timestep (Essery, 2015). Snow layer
507 temperatures are then updated using an implicit finite difference scheme. Snow compaction and density of each
508 layer are calculated in the same way as for the cryospheric layer version, as described in the following.

509 3.10 Snow density

510 For both layering schemes, fresh snow density is calculated using the temperature-dependent parameterization by
511 Anderson (1976), assuming a minimum density of 50 kg m^{-3}. Snow compaction can be calculated using two
512 methods, one physically based approach following Anderson (1976) and Jordan (1991), and one empirical
513 approach following Essery (2015). For the former, density changes are calculated in two stages due to snow

compaction and metamorphism, taking into account temperature and snow load imposed by the layers above (see also Koivusalo et al., 2001). For the empirical method, assumptions are made for maximum density of snow below 0 °C and for melting conditions (default values: 300 kg m⁻³ for cold snow and 500 kg m⁻³ for melting snow). The timescale for compaction is an adjustable parameter (default value: 200 h). The increase of density for every timestep is calculated as a fraction of the compaction timescale multiplied with the difference of maximum density and the density of the last timestep (Essery, 2015).

3.11 Liquid water content

Meltwater occuring at the snow surface is not immediately removed from the snowpack, but a certain liquid water content (LWC) can be retained. Following either Braun (1984) or Essery (2015), the maximum LWC is defined as mass fraction of SWE or as a fraction of pore volume that can be filled with liquid water (volumetric water content). If the maximum LWC is reached during snowmelt, runoff at the bottom of a snow layer occurs and drains to the snow layer underneath, or – for the bottom snow layer – into the upper soil layer respectively. In the case of a negative energy balance, this liquid water can refreeze.

3.12 Snowmelt

Snowmelt can be computed in openAMUNDSEN by several approaches with different complexity. The simplest method, the classical temperature index approach, is particularly suited for regions where only daily recordings of temperature and precipitation are available. Melt M in mm per timestep is thereby computed as:

$$M = \begin{cases} DDF \cdot T & T > T_T \\ 0 & T \leq T_T \end{cases}$$

with DDF being the degree day factor (or melt coefficient) in mm w.e. °C day⁻¹ and T the mean daily temperature in °C. T_T is the threshold temperature above which melt is assumed to occur (e.g., 1 °C). Low DDFs will be obtained for cold and dry areas, whereas high DDFs can be expected for warm and wet areas.

Second is a hybrid approach between the temperature index method and the energy balance, the so-called "enhanced temperature index method" by Pellicciotti et al. (2005). By including potential shortwave radiation and albedo these computations can also be applied to meteorological variables in hourly time steps:

$$M = \begin{cases} TF \cdot T + RF \cdot (1 - \alpha) \cdot G & T > T_T \\ 0 & T \leq T_T \end{cases}$$

where T is an hourly temperature in °C, α is albedo and G is potential incoming shortwave radiation (which is simulated as described in 3.4). TF and RF are two empirical coefficients, the temperature factor and the shortwave radiation factor, expressed in mm h⁻¹ °C⁻¹ and m² mm W⁻¹ h⁻¹. T_T is equal to 1 °C. When temperature is below T_T no melt occurs.

Melt rates using either the cryospheric layer or the multi-layer version of openAMUNDSEN also can be computed using the surface energy balance equation:

$$Q + H + E + A + B + M = 0$$

with Q being the shortwave and longwave radiation balance, H the sensible heat flux, E the latent heat flux, A the advective energy supplied by solid or liquid precipitation and B the soil heat flux. M is the energy potentially available for melt. For a detailed description of the calculation of the individual energy fluxes see Strasser (2008). A comparison of modelling results achieved with the different approaches is shown in figure 8. The temperature index approach delivers results which only show dependence on the temperature and the precipitation gradient, but no pattern affected by different radiative energy input depending on slope and aspect (figure 8a). These computations can be performed with daily time step, hence they are comparably fast and only require temperature and precipitation as meteorological input variables. Using the energy balance for computation of the accumulation and ablation processes at the snow surface, and the cryospheric layer version for the internal processes inside the snow pack, leads to a significantly more differentiated pattern of resulting snow distribution (figure 8b): The result clearly shows the effect of topography on the ablation pattern of the snow cover on this day. In figure 8c, the energy balance was combined with the multi-layer version of the model and the application of the SRF to consider the lateral snow redistribution processes. Now, erosion from exposed summit and ridge areas can be detected, as

well as additional accumulation in the slopes beneath. This complex pattern best matches the snow distribution as depicted in the fractional snow cover map derived from a Sentinel-2 image captured on the same day (figure 8d). The comparison of the simulation results achieved with increasingly sophisticated model versions shows that their plausibility clearly improves with consideration of radiative energy supply (8b) and lateral snow redistribution (8c).
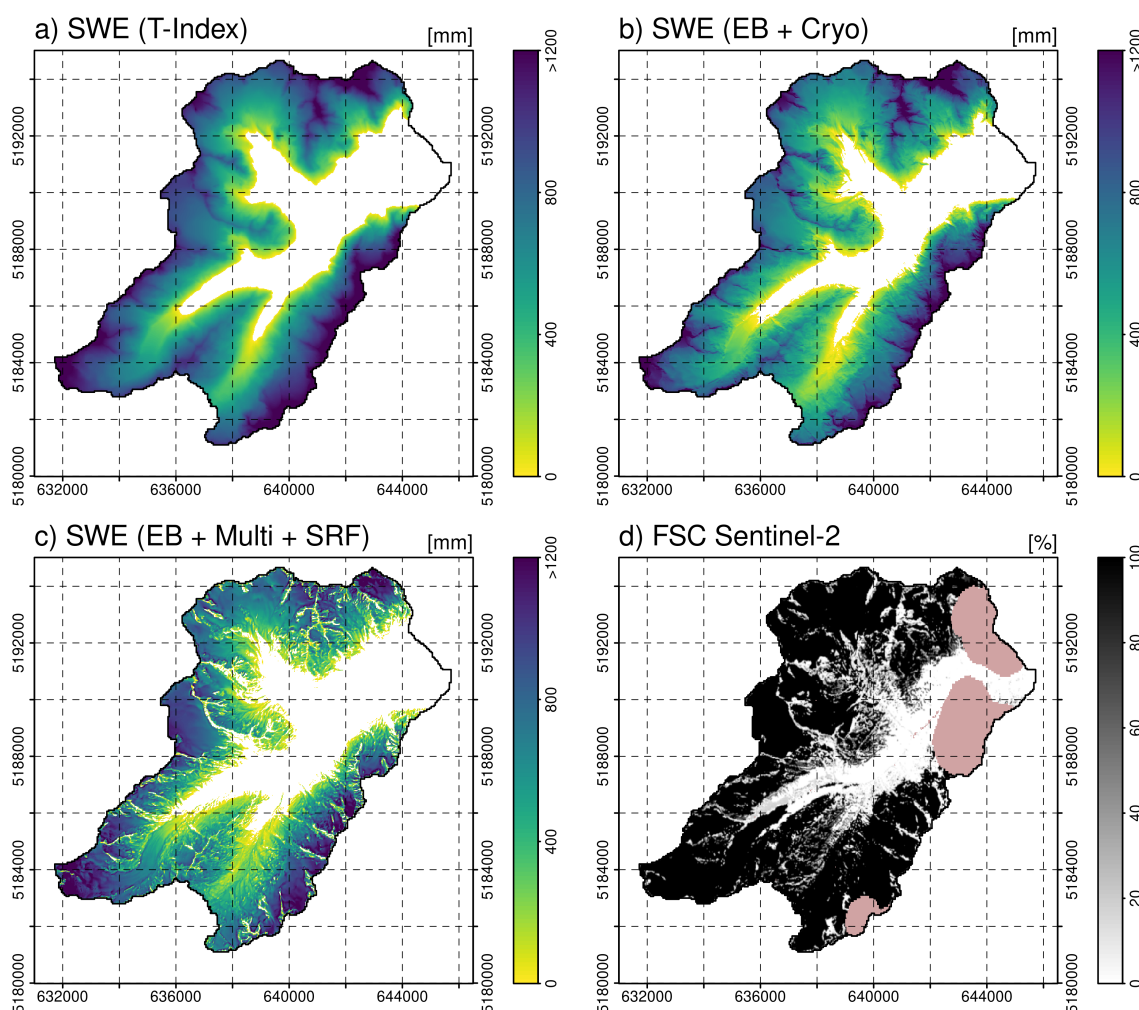
Figure 8: Snow water equivalent on 18/06/2019 in the Rofental, simulated using the temperature index approach in daily resolution without wind-induced snow redistribution (a), using the energy balance (EB) approach and cryospheric layers (Cryo) without wind-induced snow redistribution (b) and using the energy balance (EB) approach with multi-layers (Multi) including wind-induced snow redistribution (SRF) (c). Panel (d) shows a fractional snow cover (FSC; including the glacier areas) map derived from Sentinel-2 satellite data for the same day (pink bobbles are unclassified pixes, in this case clouds).

4 Implementation in Python

For the rewriting of the original AMUNDSEN IDL code the Python language was chosen due to its popularity, simplicity and the large number of excellent and well-tested numerical and scientific libraries available. openAMUNDSEN especially makes use of the packages NumPy (Harris et al., 2020) for array calculations, pandas (McKinney, 2010) and Xarray (Hoyer and Hamman, 2017) for processing time series and multidimensional data sets. While Python, being a scripting language, has limitations in terms of execution performance, these libraries allow efficient code execution due to the use of Fortran or C for the underlying calculations. For increasing the runtime efficiency of performance-critical functions within openAMUNDSEN, the Numba library (Lam et al., 2015) is furthermore used for dynamically translating Python code into machine code.

openAMUNDSEN is implemented using an object oriented architecture, centering around the `OpenAmundsen` class as the primary interface. This class represents a single model run and encapsulates all methods required to

14

582 initialize and run the model. openAMUNDSEN can either be used as a stand-alone utility (using the
583 `openamundsen` command line tool) or as a Python library. When used in stand-alone mode, the
584 `openamundsen` command line tool must be invoked with the name of a configuration file in YAML format (i.e.,
585 `openamundsen config.yml`). If used as a library from within a Python script, the model configuration in
586 form of a Python dictionary (commonly again sourced from a YAML file) must be passed when instantiating an
587 `OpenAmundsen` object. A typical model run executed from within Python looks as follows:

```
588 import openamundsen as oa
589
590 config = oa.read_config('config.yml')
591 model = oa.OpenAmundsen(config)
592 model.initialize()
593 model.run()
```

594 This allows for substantial flexibility in simulation preparation, execution and postprocessing. For example:

595 • It is possible to change the model state variables after initializing them (e.g., the snow layers – which are by
596   default initialized as being snow-free – can be initialized using prepared snow depth or SWE data). This is
597   not only possible prior to running the model, but can also be done at any point during the model run by using
598   `model.run_single()` – which performs the calculations for a single time step – in a loop, instead of the
599   `model.run()` call
600 • Model results do not necessarily have to be written to file but can also be stored in-memory and accessed
601   directly from the `OpenAmundsen` class instance for further processing
602 • Several model runs can be prepared in a single script by initializing multiple `OpenAmundsen` instances and,
603   e.g., be run in parallel.

604 Model runtime is influenced by various factors, most importantly the number of pixels simulated, but also the
605 number of weather stations used for interpolation of the meteorological variables, the choice of the layering scheme
606 (cryospheric layers vs. multi-layer), the activated submodules (snow-canopy interaction, evapotranspiration, etc.),
607 the amount of I/O operations (the number of output variables and the temporal frequency in which they are written
608 to file), and others. openAMUNDSEN generally leverages multiple CPU cores (by operating over the model grid
609 pixels in parallel using Numba's parallelization features), however in practice the speedup gained by parallelism
610 is small due to the short-lived nature of the respective functions and the overhead from scaling to multiple cores.
611 To give an example, a point-scale (i.e., 1x1) model run completes a full-year simulation using hourly time steps
612 in approx. 2 minutes on an AMD EPYC 7502P processor. A spatially distributed model run for a medium-sized
613 model grid (450 x 650 pixels) requires approx. 36 minutes per simulation year in single-core mode, and
614 33/30/28/27 minutes when using 2/4/8/16 cores, respectively. Running the model in pure Python mode (i.e.,
615 disabling the Numba just-in-time compilation) can increase runtime by a factor of more than 40.

616 5 Model uncertainty and evaluation

617 The original versions of ESCIMO and then AMUNDSEN have been extensively validated in various Alpine sites
618 (Strasser and Mauser, 2001; Strasser et al., 2002; Strasser, 2004; Pellicciotti et al., 2005; Strasser et al., 2008;
619 Strasser, 2008; Hanzer et al., 2014; Marke et al., 2015). Hanzer et al. (2016) showed the uncertainty of the model
620 application by means of a systematic, independent, complete and redundant validation procedure based on the
621 observation scale of temporal and spatial support, spacing, and extent (Blöschl, 1999). To evaluate the dimensions
622 of the observation scale a comprehensive set of eight independent validation sources was used: (i) mean areal
623 precipitation derived by conserving mass in the closure of the water balance, (ii) time series of snow depth
624 recordings at the plot scale, (iii-iv) multitemporal snow extent maps derived from Landsat and MODIS satellite
625 data products, (v) snow accumulation distribution derived from airborne laser scanning data, (vi) specific surface
626 mass balances for three glaciers in the study area, (vii) spatially distributed glacier surface elevation changes for
627 the entire area and (viii) runoff recordings for several subcatchments. By means of this evaluation procedure, both
628 the simulated spatial patterns of the snow cover, as well as time series of its evolution, are quantitatively analyzed
629 with a maximum of considered independent comparison measures; the method hence represents an unprecedented
630 completeness in the comparison of the simulation results with observations. The results indicate a high overall
631 model skill in all the dimensions and confirmed the very good model evaluations of the published case studies
632 (Hanzer et al., 2016). As an example for the model performance at the location of a meteorological station, figure
633 9 shows snow depth (9a) and SWE (9b) simulation results achieved with meteorological observations at the
634 Proviantdepot station (2737 m a.s.l.) compared to recordings of snow depth for the winter seasons 2020/2021 and
635 2021/2022. All model versions well capture the seasonal course of the snow depth evolution. Of course, the

temperature index version could be optimized by means of calibration to better match the meltout time, so the lag of some days is not a lack of model "accuracy" in this case (a standard degree day factor of 6.0 mm K^{-1} d^{-1} was used, the same as for the results in figure 8a, without further calibration). The energy balance version of the model using the multilayer approach and considering lateral snow redistribution provides the best matching representation of the observations.
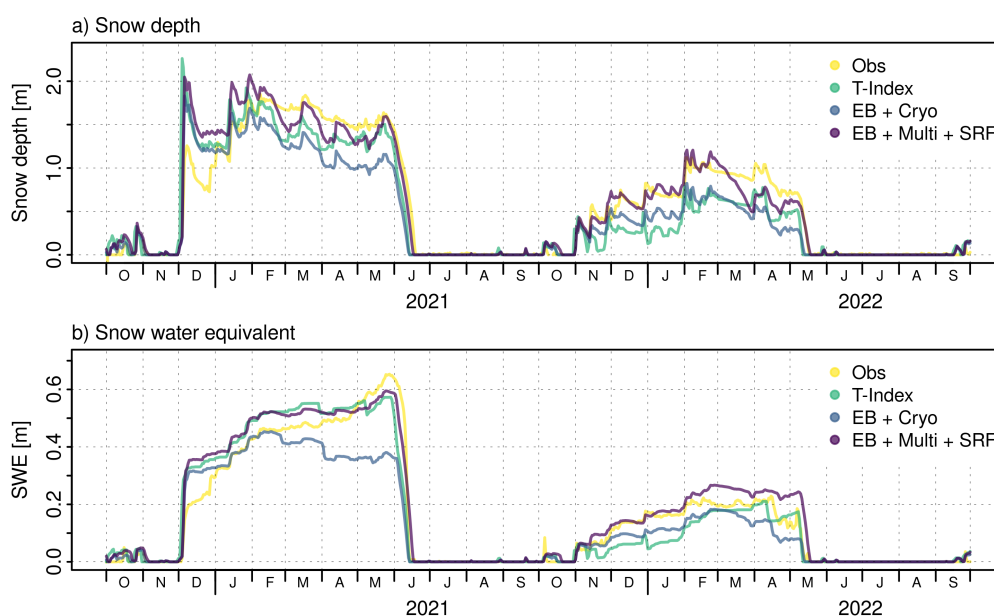
Figure 9: Observed and simulated snow depth (a) and SWE (b) at the location of the meteorological station Proviantdepot (2737 m a.s.l.) located in the area of the example application Rofental (46.82951°N, 10.82407°E) for the winter seasons 2020/2021 and 2021/2022. The Pearson correlation/Nash-Sutcliffe efficiency/Kling-Gupta efficiency/RMSE for the T-index simulations of snow depth is 0.92/0.79/0.77/0.269, and for SWE 0.96/0.93/0.94/0.055. For the EB+Cryo model version, it is 0.93/0.70/0.61/0.283 (snow depth) and 0.94/0.76/0.65/0.076 (SWE), and for the EB+Multi+SRF model simulation 0.96/0.92/0.95/0.186 (snow depth) and 0.98/0.95/0.88/0.046 (SWE), respectively.

For the multi-layer version of the openAMUNDSEN model, the uncertainty of the model simulations was investigated by Günther et al. (2019) for point simulations at the local scale and by Günther et al. (2020) for distributed applications.

openAMUNDSEN was also subject to several model intercomparison studies. The very first version of the bulk energy balance approach of AMUNDSEN (then still called ESCIMO) was compared to CROCUS for data of the Col de Porte weather station located in the French Alps (1340 m a.s.l.) (Strasser et al., 2002). Later, the model was intercompared to many other snow models in the series of the international Snow Model Intercomparison Projects (SnowMIPs): in the original SnowMIP project (Etchevers et al., 2004), ESCIMO was evaluated together with 22 other snow models of varying complexity at the point scale using meteorological observations from the two mountainous Alpine sites Col de Porte (1340 m a.s.l.) and Weissfluhjoch (2540 m a.s.l.), both in the European Alps. In the follow-up project SnowMIP2 (https://www.geos.ed.ac.uk/~ressery/SnowMIP2.html; last access: June 1, 2024), thirty-three snowpack models of varying complexity and purpose were evaluated across a wide range of hydrometeorological and forest canopy conditions at five Northern Hemisphere locations, namely (Essery et al., 2009; Rutter et al., 2009): Alptal (Switzerland; 1185 m a.s.l.), BERMS (Canada; 579 m a.s.l.), Fraser (USA; 2820 m a.s.l.), Hitsujigaoka (Japan; 182 m a.s.l.) and Hyytiälä (Finland; 181 m a.s.l.). For each location two sites were used, one in the open (no canopy) and one forested (canopy) site. Finally, the surface energy balance core of the model participated in ESM-SnowMIP (https://climate-cryosphere.org/esm-snowmip/; last access: June 1, 2024), an international intercomparison project to evaluate twenty-seven current snow models against local and global observations for a wide variety of settings, including snow schemes that are included in Earth System Models (Krinner et al., 2018). A further objective of ESM-SnowMIP is to better quantify snow-related feedbacks in the Earth system. ESM-SnowMIP is tightly linked to the Land Surface, Snow and Soil Moisture Model Intercomparison Project (https://climate-cryosphere.org/ls3mip/; last access: June 1, 2024), which is a contribution to the 6th phase of the Coupled Model Intercomparison Project (CMIP6; https://wcrp-cmip.org/cmip-phase-6-cmip6/; last access: June 1, 2024). One of the results of ESM-SnowMIP was an unexpected surprise: more sites, more years and more variables do not necessarily provide more insight into key snow processes; instead, "this led

16

to the same conclusions as previous MIPs: albedo is still a major source of uncertainty, surface exchange parameterizations are still problematic, and individual model performance is inconsistent. In fact, models are less classifiable with results from more sites, years and evaluation variables" (Menard et al., 2021). Currently, openAMUNDSEN belongs to the range of models within the COPE initiative (Common Observing Period Experiment) of the INARCH project (https://inarch.usask.ca/science-basins/cope.php; last access: June 1, 2024). It can be expected that many new insights about the models internals will mutually be learned from these model intercomparisons in the upcoming future.

6 Conclusions

In this paper, we present openAMUNDSEN, a fully distributed open source snow-hydrological model for mountain catchments. The model includes a wide range of process representations of empirical, semi-empirical and physical nature. openAMUNDSEN allows finding a compromise between temporal and spatial resolution, time span of the simulation experiment, size of the considered region, physical detail and consistency as well as performance. E.g., it offers choices between the temperature index approach to determine snowmelt rates from daily temperature and precipitation, or hourly closure of the surface energy balance and calculation of a number of state variables for several snow layers using temperature, precipitation, humidity, radiation and wind speed as forcing data. openAMUNDSEN is computationally efficient, of modular nature, easily extendible and also allows for using factorial designs to determine interactions between processes and their effect on the accuracy of the simulation results (Essery et al., 2013; Günther et al., 2019, 2020). Hence, the application of the model is very flexible and it supports a multitude of applications or simulation experiments to address any kind of hydrological, glaciological, climatological or related research questions.

The model has been evaluated and proven its applicability at many sites worldwide. Most of all, it was subject to a systematic, innovative, multilevel spatiotemporal validation with independent datasets of various resolution and extent from an instrumented site in the European Alps (Hanzer et al., 2016). In all cases, the model showed high overall skill and well captured the spatial and temporal patterns as well as magnitudes of the observations.

The Python model code for openAMUNDSEN is available for the public as open source project on GitHub (https://github.com/openamundsen/openamundsen; last access: June 1, 2024), including a documentation which is subject to continuous extension and improvement (https://doc.openamundsen.org; last access: June 1, 2024). The bootstrap resampling weather generator (see Appendix) is available at https://github.com/openamundsen/openamundsen-climategenerator (last access: June 1, 2024).

7 Future developments

The openAMUNDSEN model code is continuously further improved and extended. The modelling of the processes of lateral snow redistribution will benefit from a simulation of local wind fields, e.g. as recently demonstrated by Quéno et al. (2023). On top of the wind-induced processes of saltation, turbulent suspension (with sublimation) snow is also transported downslope by means of avalanches, the origin also of accumulated masses of snow leewards of crests. In the original, IDL-based version of AMUNDSEN (Strasser, 2008) the avalanche process was parameterized based on the Mflow-TD algorithm by Gruber (2007); the latter was later extended with a continuous update of the surface elevation model to correct for eroded/deposited masses of snow (Bernhardt and Schulz, 2010). A comparable algorithm is in development to be included in openAMUNDSEN soon. Another path of improvement is foreseen for the snow-canopy interaction module. On the one hand, the parameterization of inside-canopy meteorological variables derived from measurements taken in the open will be further improved by utilizing the new (winter) measurements of inside-canopy meteorological variables, i.e. from the Col de Porte meteorological station in the French Alps (Sicart et al., 2023). Further, it is intended to couple the snow-canopy interaction module with a dynamically simulated evolution of the LAI from iLand model simulations (Seidl et al., 2012). The ultimate goal of this effort is to bi-directionally couple the snow processes inside the canopy with its long-term evolution to enable the simulation of scenarios of the effect of climate change on the coupled hydrological/biological system of mountain forests.

To compute streamflow discharge in mostly glacierized catchment to be compared to gauge recordings, a linear reservoir cascade approach following Asztalos (2007) has been implemented as a separate post-processing tool (Hanzer et al., 2016). The linear reservoir approach is a comparable simple empirical method to produce a runoff curve for a certain location of the stream without the need to provide physical parameters for the catchment characteristics (e.g., soil), or the wave propagation along the channel. Instead, a series of parallel linear reservoir cascades (Nash, 1960) is computed the parameters of which are calibrated by maximizing the Nash-Sutcliffe efficiency NSE and minimizing the relative volume error (following Lindström, 1997). Due to its purely empirical

nature and the fact that its application is limited to small glacierized catchments with short concentration time only, the linear reservoir approach will not be included into the openAMUNDSEN project on the openAMUNDSEN GitHub repository. Instead, it is foreseen to test and develop new approaches in machine learning, e.g. in the field of LSTM (Long Short-Term Memory Networks Modelling) which can provide very good results for hydrological streamflow simulations (Kratzert et al., 2021). Other such new developments also exist in the combination of hydrologial modelling, remote sensing and machine learning (De Gregorio et al., 2019a and b). Since AI is a field of rapid development in scientific modelling we expect significant advances also in snow-hydrological modelling using these innovative methods.

Finally, we see a promising way to increase the model accuracy by assimilating satellite data derived maps of, e.g., snow coverage and/or wet snow area to select the best matching model run out of an ensemble of simulations that has been created by perturbating the meteorological forcing or the parameters of the model. First developments are already undertaken in this direction. This way the model can also be accurately initialized when applied for predictions using weather forecast model output as meteorological forcing.

Appendix: Generation of potential future climate in openAMUNDSEN

Data timeseries of future climate evolution to force openAMUNDSEN for climate change scenario simulations can be produced by means of a stochastic block bootstrap resampler which is realized as external pre-processing routine (https://github.com/openamundsen/openamundsen-climategenerator; last access June 1, 2024). The method requires a sufficiently long time series of historical meteorological recordings from a period with as much as possible variable weather conditions in the considered region. The principles of the implemented weather generator follow Strasser (2008) and are described herein. Basic assumption of the method is that a climate storyline can be divided into time periods which are characterized by a certain mean temperature and precipitation and that these two variables are not independent from each other:

$$P_{tot} = f\,(T_{mean})$$

Thereby P_{tot} is the total precipitation amount of a specific time period, T_{mean} is the mean temperature and f their functional dependency. The time periods can be set to any length, i.e. to months as in Mauser et al. (2007) or to weeks as in Strasser (2008). In a first step, the typical annual course of the measured meteorological variables is constructed by computing mean temperature and total precipitation for the periods using all years of the historical dataset and applying the given formula. Whereas temperature is characterized by a typical seasonal course in the Alpine region (warm in summer, cold in winter), the annual course of the precipitation totals of a period with certain duration can be more complex. The resulting mean annual climate course is used to construct the future data time series period by period: firstly, the respective temperature for the period is modified with a random variation factor and an assumed projected temporal trend (e.g., as derived from a regional climate model application). Then a corresponding precipitation is derived and, again, a random variation. In the end the climate of a future period is defined by the so obtained mean temperature and precipitation. In a final step, the period from the historical pool having the most similar temperature and precipitation is selected by applying an Euclidian nearest neighbour distance measure. All respective data of the chosen period (e.g. air temperature, precipitation, global radiation, relative humidity and wind speed) are then added to the future time series to be constructed. This procedure is continuously repeated for all periods of the year, and for all years of the future time series. By modifying the applied random variation a change in climate variability can be simulated. To allow for more flexibility in the construction of the periods, in our implementation the basic population from which the measured period is chosen (= the number of periods available, being equal to the number of years for which observational data is available) can be synthetically extended by allowing for one or more periods before and after the one to be constructed (figure A1).
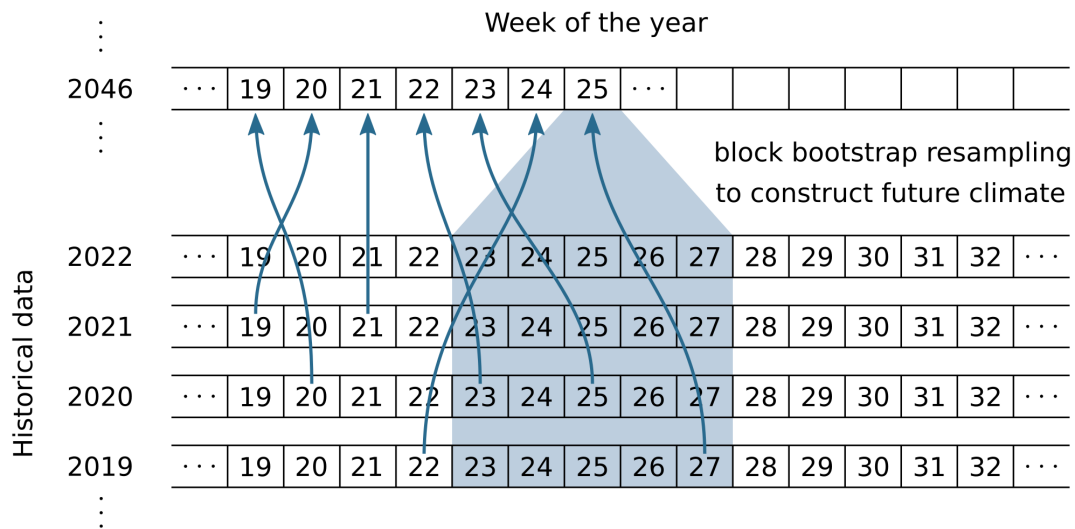
Figure A1: openAMUNDSEN pre-processing with the weather generator: choice of corresponding historical periods to construct a data timeseries of future climate evolution with preset trend and random variation from given meteorological observations. The number of periods from which data can be selected to construct a particular period of a year in the future time series is set to five in this example.

The described procedure has a number of specific features: (i) the key advantage of the method is that the physical relationship between the meteorological variables is maintained in the simulation; (ii) bootstrap models, such as the described one, obviously work well at high temporal resolution, e.g. 1 to 3-hourly; (iii) the produced data time series is in the validated range for the subsequent hydrological modelling; (iv) a synthetic baseline scenario can easily be constructed by assuming a zero trend for temperature; (v) the procedure is computationally very efficient and finally, (vii) the spatial resolution of the data is preserved as it exactly corresponds to the weather station locations. However, a significant drawback of the method is that auto-correlation between the periods is lost and the consideration of changes in the variability of the meteorological variables is limited. Together with the fact that changes in extreme values are not considered (only their frequency can change) it becomes clear that the data resulting from the method cannot be used for modelling variations in the extent of hydrological extremes. Furthermore and most crucial, no coupling is considered between the (simulated) characteristics of the land surface – e.g. whether it is snow-covered or not – and the atmosphere, and therefore the important effects of feedback mechanisms are not conserved in the construction of the data timeseries. This, however, is a drawback that also many physical climate models share. Examples of the application of the procedure to the high Alpine region of the Berchtesgaden Alps (Germany) with subsequent modelling of snow processes, including snow-canopy interaction, are given in Strasser (2008).

Code availability.

The openAMUNDSEN model code is available under the MIT license, a short and simple permissive license with conditions only requiring preservation of copyright and license notices. The download site for the model code is https://github.com/openamundsen/openamundsen (last access: June 1, 2024). The model in the presented version v1.0 is available on Zenodo (Hanzer et al., 2024).

Data availability.

We provide a comprehensive data set that can be used with openAMUNDSEN for the high alpine research catchment of the upper Rofenache (98.1 km^2, Ötztal Alps, Tyrol/Austria) under the Creative Commons Attribution License at PANGAEA (https://doi.org/10.1594/PANGAEA.876120; last access: June 1, 2024) including (i) glaciological data, i.e., recordings of glacier volume and geometry changes; (ii) meteorological data as recorded by temporally installed or permanent automatic weather stations; (iii) hydrological data characterizing the water balance of the respective glaciated (sub-) catchment; and (iv) airborne and terrestrial laser scanning data (Strasser et al. 2018). The data time series cover periods of various lengths until 2017. This data is currently extended until August 2023 under the same license (Warscher et al., 2024) and available at https://doi.org/10.5880/fidgeo.2023.037 (last access: July 21, 2024).

Sample availability.

819   *Competing interests.*

820   The authors declare that no competing interests exist.

821   *Disclaimer.*

822   TEXT

854   References

855   Allen, R. G., Pereira, L. S., Raes, D. and Smith, M.: Crop evapotranspiration - Guidelines for computing crop
856   water requirements. FAO Irrigation and Drainage Paper No. 56, 174 p. ISBN 92-5-104219-5,
857   https://www.fao.org/3/x0490e/x0490e00.htm, 1998.

858   Anderson, E. A.: A point energy and mass balance model of a snow cover. NOAA Technical Report NWS 19, pp.
859   1–172, https://repository.library.noaa.gov/view/noaa/6392, 1976.

860   Asztalos, J., Kirnbauer, R., Escher-Vetter, H. and Braun, L.: A distributed energy balance snowmelt model as a
861   component of a flood forecasting system for the Inn river. In: Strasser, U. and Vogel M. (eds.) (2008): Proceedings
862   of the Alpine*Snow*Workshop, Munich, October 5–6, 2006, Germany. Research report 53, ISBN13 978-3-
863   922325-60-4, National Park Berchtesgaden, 2007.

864   Barnes, S. L.: A technique for maximising details in numerical weather map analysis. J. Appl. Meteor., 3, pp. 396–
865   409, 1964.

866   Barnett, T. P., Adam, J. C. and Lettenmaier, D. P.: Potential impacts of a warming climate on water availability in
867   snow- dominated regions. Nature, 438, pp. 303–309, https://doi.org/10.1038/nature04141, 2015.

868   Bavay, M. and Egger, T.: MeteoIO 2.4.2: a preprocessing library for meteorological data. Geosci. Model. Dev.
869   Vol. 8, pp. 3135–3151, https://doi.org/10.5194/gmd-7-3135-2014, 2014.

870   Bernhardt, M. and Schulz, K.: SnowSlide: A simple routine for calculating gravitational snow transport. Geophys.
871   Res. Lett., Vol. 37, L11 502, https://doi.org/10.1029/2010GL043086, 2010.

872   Blöschl, G.: Scaling issues in snow hydrology. Hydrol. Process., Vol. 13, pp. 2149–2175, 1999.

873   Blöschl, G. and Kirnbauer, R.: Point snowmelt models with different degrees of complexity–internal processes. J.
874   Hydrol., Vol. 129, pp. 127–147, https://doi.org/10.1016/0022-1694(91)90048-M, 1991.

875   Braun, L. N.: Simulation of snowmelt-runoff in lowland and lower alpine regions of Switzerland. Ph.D. thesis,
876   ETH Zurich, 1984.

877   Corripio, J.: Vectorial algebra algorithms for calculating terrain parameters from DEMs and solar radiation
878   modelling in mountainous terrain. Int. J. Geogr. Inf. Sci., Vol. 17(1), pp. 1–23, https://doi.org/10.1080/713811744,
879   2003.

880   De Gregorio, L., Günther, D., Callegari, M., Strasser, U., Zebisch, M., Bruzzone, L. and Notarnicola, C.:
881   Improving SWE Estimation by Fusion of Snow Models with Topographic and Remotely Sensed Data. Rem. Sens.,
882   11(17), 2033, https://doi.org/10.3390/rs11172033, 2019a.

883   De Gregorio, L., Callegari, M., Marin, C., Zebisch, M., Bruzzone, L., Demir, B., Strasser, U., Marke, T., Günther,
884   D., Nadalet, R. and Notarnicola, C.: A novel data fusion technique for snow cover retrieval. J. Sel. Top. Appl.
885   Earth Obs. Rem. Sens. JSTARS, Vol. 12, No. 8, https://doi.org/10.1109/JSTARS.2019.2920676, 2019b.

886   Ebner, P. P., Koch, F., Premier, V., Marin, C., Hanzer, F., Carmagnola, C. M., Hugues, F., Günther, D., Monti, F.,
887   Hargoaa, O., Strasser, U., Morin, S. and Lehning, M.: Evaluating a prediction system for snow management. The
888   Cryosphere, https://doi.org/10.5194/tc-15-3949-2021, 2021.

889   Essery, R., Rutter, N., Pomeroy, J., Baxter, R., Staehli, M., Gustafsson, D., Barr, A., Bartlett, P. and Elder, K.:
890   SNOWMIP2: An evaluation of forest snow process simulations. Bull. Am. Met. Soc., 90 (8), pp. 1120–1136,
891   https://doi.org/10.1175/2009BAMS2629.1, 2009.

892   Essery, R., Morin, S., Lejeune, Y. and Ménard C. B.: A comparison of 1701 snow models using observations from
893   an alpine site. Adv. Wat. Res. 55, pp.131–148, https://doi.org/10.1016/j.advwatres.2012.07.013, 2013.

894 Essery, R.: A factorial snowpack model (FSM 1.0). Geosci. Model. Dev. 8, pp. 3867–3876,
895 https://doi:10.5194/gmd-8-3867-2015, 2015.

896 Etchevers, P., Martin, E., Brown, R., Fierz, C., Lejeune, Y., Bazile, E., Boone, A., Dai, Y.-J., Essery, R. L. E.,
897 Fernandez, Y., Gusev, Y., Jordan, R., Foren, V., Kowalczyk, E., Nasonova, N. O., Pyles, R. D., Schlosser, A.,
898 Shmakin, A. B., Smirnova, T. G., Strasser, U., Verseghy, D., Yamazaki, T. and Yang, Z.-L.: Validation of the
899 surface energy budget simulated by several snow models (SnowMIP project). Ann. Glaciol., Vol. 38, pp. 150–
900 158, https://doi.org/10.3189/172756404781814825, 2004.

901 Fischer, A., Seiser, B., Stocker-Waldhuber, M., Mitterer, C. and Abermann, J.: Tracing glacier changes in Austria
902 from the Little Ice Age to the present using a lidar-based high-resolution glacier inventory in Austria. The
903 Cryosphere, 9(2), pp. 753–766, https://doi.org/10.5194/tc-9-753-2015, 2015.

904 Förster, K., Hanzer, F., Winter, B., Marke, T. and Strasser, U.: MELODIST – An open-source MeteoroLOgical
905 observation time series DISaggregation Tool. Geosci. Model Dev., Vol. 9, pp. 2315–2333,
906 https://doi.org/10.5194/gmd-9-2315-2016, 2016.

907 Freudiger, D., Kohn, I., Seibert, J., Stahl, K. and Weiler, M.: Snow redistribution for the hydrological modeling
908 of alpine catchments. WIREs Water, e1232, pp. 1–16, https://doi.org/10.1002/wat2.1232, 2017.

909 Goodison, B. E., Louie, P. and Yang, D.: WMO solid precipitation measurement intercomparison. Tech. Rep.
910 WMO/TD 872, Geneva, 1998.

911 Gruber, S.: A mass-conserving fast algorithm to parameterize gravitational transport and deposition using digital
912 elevation models. Water Resour. Res., Vol. 43, W06412, https://doi.org/10.1029/2006WR004868, 2007.

913 Grünewald, T., Stötter, J., Pomeroy, J. W., Dadic, R., Moreno Baños, I., Marturià, J., Spross, M., Hopkinson, C.,
914 Burlando, P. and Lehning, M.: Statistical modelling of the snow depth distribution in open alpine terrain. Hydrol.
915 Earth Syst. Sci., Vol. 17, pp. 3005–3021, https://doi.org/10.5194/hess-17-3005-2013, 2013.

916 Grünewald, T., Bühler, Y. and Lehning, M.: Elevation dependency of mountain snow depth. The Cryosphere, 8,
917 pp. 2381–2394, https://doi.org/10.5194/tc-8-2381-2014, 2014.

918 Günther, D., Marke, T., Essery, R. and Strasser, U.: Uncertainties in Snowpack Simulations – Assessing the Impact
919 of Model Structure, Parameter and Forcing Data Error on Point-Scale Energy-Balance Snow Model Performance.
920 Water Resour. Res., Vol. 55, pp. 2779–2800, https://doi.org/10.1029/2018WR023403, 2019.

921 Günther, D., Hanzer, F., Warscher, M., Essery, R. and Strasser, U.: Including parameter uncertainty in an
922 intercomparison of physically-based snow models. Front. Earth Sci., Vol. 8, 542599,
923 https://doi.org/10.3389/feart.2020.542599, 2020.

924 Hanzer, F., Marke, T. and Strasser, U.: Distributed, explicit modelling of technical snow production for a ski area
925 in the Schladming Region (Austrian Alps). Cold Reg. Sci. Technol., Vol. 108, pp. 113–124,
926 https://doi.org/10.1016/j.coldregions.2014.08.003, 2014.

927 Hanzer, F., Helfricht, K., Marke, T. and Strasser, U.: Multi-level spatiotemporal validation of snow/ice mass
928 balance and runoff modeling in glacierized catchments. The Cryosphere, Vol. 10, pp. 1859–1881,
929 https://doi.org/10.5194/tc-10-1859-2016, 2016.

930 Hanzer, F., Förster, K., Nemec, J. and Strasser, U.: Projected hydrological and cryospheric impacts of 21st century
931 climate change in the Ötztal Alps (Austria) simulated using a physically based approach. Hydrol. Earth Syst. Sci.,
932 Vol. 22, pp. 1593–1614, https://dx.doi.org/10.5194/hess-22-1593-2018, 2018.

933 Hanzer, F., Carmagnola, C. M., Ebner, P. P., Koch, F., Monti, F., Bavay, M., Bernhardt, M., Lafaysse, M.,
934 Lehning, M., Strasser, U., François, H. and Morin, S.: Simulation of snow management in Alpine ski resorts using
935 three different snow models. Cold Reg. Sci. Technol., Vol. 172, 102995,
936 https://doi.org/10.1016/j.coldregions.2020.102995, 2020.

937 Hanzer, F., Warscher, M. and Strasser, U.: openAMUNDSEN v1.0.0 (v1.0.0). Zenodo.
938 https://doi.org/10.5281/zenodo.11859175, 2024.

939 Harris, C. R., Millman, K. J., van der Walt, S. J., Gommers, R., Virtanen, P., Cournapeau, D., Wieser, E., Taylor,
940 J., Berg, S., Smith, N. J., Kern, R., Picus, M., Hoyer, S., van Kerkwijk, M. H., Brett, M., Haldane, A., del Río, J.
941 F., Wiebe, M., Peterson, P., Gérard-Marchant, P., Sheppard, K., Reddy, T., Weckesser, W., Abbassi, H., Gohlke,
942 C. and Oliphant, T. E.: Array programming with NumPy. Nature, 585(7825), 7825,
943 https://doi.org/10.1038/s41586-020-2649-2, 2020.

944 Huss, M. and Farinotti, D.: Distributed ice thickness and volume of all glaciers around the globe. J. Geophys. Res.
945 Earth Surface, Vol. 117, F04010, https://doi.org/10.1029/2012JF002523, 2012.

946 Helfricht, K.: Analysis of the spatial and temporal variation of seasonal snow accumulation in Alpine catchments
947 using airborne laser scanning. Ph.D. thesis, Innsbruck, 2014.

948 Hoyer, S. and Hamman, J.: xarray: N-D labeled Arrays and Datasets in Python. Journal Open Res. Soft., 5(1),
949 https://doi.org/10.5334/jors.148, 2017.

950 Kochendorfer, J., Rasmussen, R., Wolff, M., Baker, B., Hall, M. E., Meyers, T., Landolt, S., Jachcik, A., Isaksen,
951 K., Brækkan, R. and Leeper, R.: The quantification and correction of wind-induced precipitation measurement
952 errors. Hydrol. Earth Syst. Sci., 21(4), pp. 1973–1989, https://doi.org/10.5194/hess-21-1973-2017, 2017.

953 Koivusalo, H., Heikinheimo, M. and Karvonen, T.: Test of a simple two-layer parameterisation to simulate the
954 energy balance and temperature of a snow pack. Theor. Appl. Clim., 70(1–4), pp. 65–79,
955 https://doi.org/10.1007/s007040170006, 2001.

956 Kratzert, F., Gauch, M., Nearing, G., Hochreiter, S. and Klotz, D.: Niederschlags-Abfluss-Modellierung mit Long
957 Short-Term Memory (LSTM). Österr. Wasser- und Abfallw., https://doi.org/10.1007/s00506-021-00767-z, 2021.

958 Krinner, G., Derksen, C., Essery, R., Flanner, M., Hagemann, S., Clark, M., Hall, A., Rott, H., Brutel-Vuilment,
959 C., Kim, H., Ménard, C., Mudryk, L., Thackeray, C., Arduini, G., Bartlett, P., Boone, A., Chéruy, F., Colin, J.,
960 Cuntz, M., Dai, Y., Decharme, B., Derry, J., Ducharne, A., Dutra, E., Fang, X., Fierz, C., Ghattas, J., Gusev, Y.,
961 Haverd, V., Kontu, A., Lafaysse, M., Law, R., Lawrence, D., Li, W., Marke, T., Marks, D., Nasonova, O., Nitta,
962 T., Niwano, M., Pomeroy, J., Raleigh, M. S., Schaedler, G., Semenov, V., Smirnova, T., Stacke, T., Strasser, U.,
963 Svenson, S., Turkov, D., Wang, L., Wang, T., Wever, N., Yuan, H. and Zhou, W.: ESM-SnowMIP: Assessing
964 models and quantifying snow-related climate feedbacks. Geosci. Model Dev., pp. 5027–5049,
965 https://doi.org/10.5194/gmd-11-5027-2018, 2018.

966 Lam, S. K., Pitrou, A. and Seibert, S.: Numba: A llvm-based python jit compiler. Proceedings of the Second
967 Workshop on the LLVM Compiler Infrastructure in HPC, pp. 1–6, 2015.

968 Lam, R., Sanchez-Gonzalez, A., Wilson, M., Wirnsberger, P., Fortunato, M., Alet, F., Ravuri, S., Ewalds, T.,
969 Eaton-Rosen, Z., Hu, W., Merose, A., Hoyer, S., Holland, G., Vinyals, O., Stott, J., Pritzel, A., Mohamed, S. and
970 Battaglia, P.: Learning skillfull medium-range global weather forecasting. Science 382, pp. 1416–1421,
971 https://www.science.org/doi/10.1126/science.adi2336, 2023.

972 Lehning, M., Bartelt, P., Brown, B., Russi, T., Stockli, U. and Zimmerli, M.: SNOWPACK model calculations for
973 avalanche warning based upon a new network of weather and snow stations. Cold Reg. Sci. Technol., Vol. 30, pp.
974 145–157, https://doi.org/10.1016/S0165-232X(99)00022-1, 1999.

975 Lindström, G.: A Simple Automatic Calibration Routine for the HBV Model. Nord. Hydrol., Vol. 28, pp. 153–
976 168, ISSN 0029-1277, E-ISSN 1996-9694, 1997.

977 Liston, G. E. and Elder, K.: A meteorological distribution system for high-resolution terrestrial modeling
978 (MicroMet). J. Hydrometeor., 7(2), pp. 217–234, https://doi.org/10.1175/JHM486.1, 2006.

979 Marke, T.: Development and Application of a Model Interface To couple Land Surface Models with Regional
980 Climate Models For Climate Change Risk Assessment In the Upper Danube Watershed. Dissertation, Ludwig-
981 Maximilians-Universität München, 188 p., München. https://doi.org/10.5282/edoc.9162, 2008.

982 Marke, T., Strasser, U., Hanzer, F., Wilcke, R., Gobiet, A. and Stötter, J.: Scenarios of future snow conditions in
983 Styria (Austrian Alps). J. Hydrometeor., Vol. 16, pp. 261–277, https://doi.org/10.1175/JHM-D-14-0035.1, 2015.

984 Marke, T., Mair, E., Förster, K., Hanzer, F., Garvelmann, J., Pohl, S., Warscher, M. and Strasser, U.:
985 ESCIMO.spread (v2): Parameterization of a spreadsheet-based energy balance snow model for inside-canopy
986 conditions, Geosci. Model Dev., Vol. 9, pp. 633–646, https://doi.org/10.5194/gmd-9-633-2016, 2016.

987 Marke, T., Hanzer, F., Olefs, M. and Strasser, U.: Simulation of Past Changes in the Austrian Snow Cover 1948–
988 2009. J. Hydrometeor., Vol. 19, pp. 1529–1545, https://doi.org/10.1175/JHM-D-17-0245.1, 2018.

989 Mauser, W., Prasch, M. and Strasser, U.: Physically based Modelling of Climate Change Impact on Snow Cover
990 Dynamics in Alpine Regions using a Stochastic Weather Generator. Proceedings of the International Congress on
991 Modelling and Simulation MODSIM07 2007, Christchurch, New Zealand, 2007.

992 McKinney, W.: Data Structures for Statistical Computing in Python. Proceedings of the 9th Python in Science
993 Conference, pp. 56–61, https://doi.org/10.25080/Majora-92bf1922-00a, 2010.

994 Menard, C., Essery, R., Krinner, G., Arduini, G., Bartlett, P., Boone, A., Brutel-Vuilmet, C., Burke, E., Cuntz, M.,
995 Dai, Y., Decharme, B., Dutra, E., Fang, L., Fierz, C., Gusev, Y., Hagemann, S., Haverd, V., Kim, H., Lafaysse,
996 M., Marke, T., Nasonova, O., Nitta, T., Niwano, M., Pomeroy, J., Schaedler, G., Semenov, V., Smirnova, T.,
997 Strasser, U., Swenson, S., Turkov, D., Wever, N. and Yuan, H.: Scientific and human errors in a snow model
998 intercomparison. Bull. Amer. Meteor. Soc., https://doi.org/10.1175/BAMS-D-19-0329.1, 2021.

999 Mott, R., Winstral, A., Cluzet, B., Helbig, N., Magnusson, J., Mazzotti, G., Quéno, L., Schirmer, M., Webster, C.
1000 and Jonas, T.: Operational snow-hydrological modeling for Switzerland. Front. Earth Sci., 11:1228158,
1001 https://doi.org/10.3389/feart.2023.1228158, 2023.

1002 Nash, J. E.: A unit hydrograph study, with particular reference to British catchments. Proc. Inst. Civ. Eng., Vol.
1003 17, pp. 249–282, 1960.

1004 Ohmura, A.: Physical basis for the temperature–based melt–index method. J. Appl. Meteor., Vol. 40, pp. 753–761,
1005 2001.

1006 Pellicciotti, F., Brock, B., Strasser, U., Burlando, P., Funk, M. and Corripio, J.: An enhanced temperature-index
1007 glacier melt model including shortwave radiation balance: development and testing for Haut Glacier D'Arolla,
1008 Switzerland. J. Glaciol., Vol. 51, Nr. 175, pp. 573–587, https://doi.org/10.3189/172756505781829124, 2005.

1009 Pfeiffer, J., Zieher, T., Schmieder, J., Rutzinger, M. and Strasser, U.: Spatio-temporal assessment of the
1010 hydrological drivers of an active deep-seated gravitational slope deformation – the Vögelsberg landslide in Tyrol
1011 (Austria). Earth Surf. Proc. Landf., http://doi.org/10.1002/esp.5129, 2021.

1012 Podsiadło, I., Paris, C., Callegari, M., Marin, C., Günther, D., Strasser, U., Notarnicola, C. and Bruzzone, L.:
1013 Integrating models and remote sensing data for distributed glacier mass balance estimation. J. Sel. Top. Appl.
1014 Earth Obs. Rem. Sens. JSTARS, Vol. 13, pp. 6177–6194, https://doi.org/10.1109/JSTARS.2020.3028653, 2020.

1015 Quéno, L., Mott, R., Morin, P., Cluzet, B., Mazzotti, G. and Jonas, T.: Snow redistribution in an intermediate-
1016 complexity snow hydrology modelling framework. EGUsphere [preprint], https://doi.org/10.5194/egusphere-
1017 2023-2071, 2023.

1018 Rasmussen, R., Baker, B., Kochendorfer, J., Meyers, T., Landolt, S., Fischer, A. P., Black, J., Thériault, J. M.,
1019 Kucera, P., Gochis, D., Smith, C., Nitu, R., Hall, M., Ikeda, K. and Gutman, E.: How well are we measuring snow?
1020 The NOAA/FAA/NCAR Winter Precipitation Test Bed. Bull. Am. Met. Soc., pp. 811–829.
1021 https://doi.org/10.1175/BAMS-D-11-00052.1, 2012.

Rohrer, M. B.: Die Schneedecke im schweizerischen Alpenraum und ihre Modellierung. Zürcher Geographische Schriften, 49, 178, 1992.

Rutter, N., Essery, R. L. E., Pomeroy, J., Altimir, N., Andreadis, K., Baker, I., Barr, A., Bartlett, P., Elder, K., Ellis, C., Feng, X., Gelfan, A., Goodbody, G., Gusev, Y., Gustafsson, D., Hellström, R., Hirota, T., Jonas, T., Koren, V., Li, W.-P., Luce, C., Martin, E., Nasonova, O., Pumpanen, J., Pyles, D., Samuelsson, P., Sandells, M., Schädler, G., Shmakin, A., Smirnova, T., Stähli, M., Stöckli, R., Strasser, U., Su, H., Suzuki, K., Takata, K., Tanaka, K., Thompson, E., Vesala, T., Viterbo, P., Wiltshire, A., Xue, Y. and Yamazaki, T.: Evaluation of forest snow processes models (SnowMIP2). J. Geophys. Res., 114, D06111, https://doi.org/10.1029/2008JD011063, 2009.

Sauter, T., Arndt, A. and Schneider, C.: COSIPY v1.3 – an open-source coupled snowpack and ice surface energy and mass balance model. Geosci. Model Dev., Vol. 13, pp. 5645–5662, https://doi.org/10.5194/gmd-13-5645-2020, 2020.

Seibert, J. and Bergström, S.: A retrospective on hydrological catchment modelling based on half a century with the HBV model. Hydrol. Earth Syst. Sci., Vol. 26, pp. 1371–1388, https://doi.org/10.5194/hess-26-1371-2022, 2022.

Seidl, R., Rammer, W., Scheller, R. M. and Spies, T. A.: An individual-based process model to simulate landscape-scale forest ecosystem dynamics. Ecol. Mod., Vol. 231, https://doi.org/10.1016/j.ecolmodel.2012.02.015, 2012.

Sicart, J. M., Ramseyer, V., Picard, G., Arnaud, L., Coulaud, K., Freche, G., Soubeyrand, D., Lejeune, Y., Dumont, M., Gouttevin, I., Le Gac, E., Berger, F., Monnet, J.-M., Borgniet, L., Mermin, E., Rutter, N., Webster, C. and Essery, R.: Snow accumulation and ablation measurements in a midlatitude mountain coniferous forest (Col de Porte, France, 1325 m altitude): the Snow Under Forest (SnoUF) field campaign data set. Earth Syst. Sci. Data, Vol. 15, https://doi.org/10.5194/essd-15-5121-2023, 2023.

Strasser, U. and Mauser, W.: Modelling the Spatial and Temporal Variations of the Water Balance for the Weser Catchment 1965–1994. J. Hydrol., Vol. 254/1-4, pp. 199–214, https://doi.org/10.1016/S0022-1694(01)00492-9, 2001.

Strasser, U., Etchevers, P. and Lejeune, Y.: Intercomparision of two Snow Models with Different Complexity Using Data from an Alpine Site. Nordic Hydrol., 33 (1), pp. 15–26, https://doi.org/10.2166/nh.2002.0002, 2002.

Strasser, U., Corripio, J., Brock, B., Pellicciotti, F., Burlando, P. and Funk, M. (2004): Spatial and Temporal Variability of Meteorological Variables at Haut Glacier d'Arolla (Switzerland) During the Ablation Season 2001: Measurements and Simulations. J. Geophys. Res., Vol. 109, D03103, https://doi.org/10.1029/2003JD003973, 2004.

Strasser, U.: Die Modellierung der Gebirgsschneedecke im Nationalpark Berchtesgaden. Modelling of the mountain snow cover in the Berchtesgaden National Park. Berchtesgaden National Park research report, Nr. 55, ISBN 978-3-922325-62-8, Berchtesgaden, 2008.

Strasser, U., Bernhardt, M., Weber, M., Liston, G. E. and Mauser, W.: Is snow sublimation important in the alpine water balance? The Cryosphere, Vol. 2, pp. 53–66, https://doi.org/10.5194/tc-2-53-2008, 2008.

Strasser, U. and Marke, T.: ESCIMO.spread - a spreadsheet-based point snow surface energy balance model to calculate hourly snow water equivalent and melt rates for historical and changing climate conditions. Geosci. Model Dev., Vol. 3, pp. 643–652, https://doi.org/10.5194/gmd-3-643-2010, 2010.

Strasser, U., Warscher, M. and Liston, G. E.: Modelling snow-canopy processes on an idealized mountain. J. Hydrometeor. Vol. 12, No. 4, pp. 663–677, https://doi.org/10.1175/2011JHM1344.1, 2011.

Strasser, U., Marke, T., Braun, L., Escher-Vetter, H., Juen, I., Kuhn, M., Maussion, F., Mayer, C., Nicholson, L., Niedertscheider, K., Sailer, R., Stötter, J., Weber, M. and Kaser, G.: The Rofental: a high Alpine research basin (1890–3770 m a.s.l.) in the Ötztal Alps (Austria) with over 150 years of hydrometeorological and glaciological observations. Earth Syst. Sci. Data, Vol. 10, pp. 151–171, https://doi.org/10.5194/essd- 10-151-2018, 2018.

Vionnet, V., Brun, E., Morin, S., Boone, A., Faroux, S., Le Moigne, P., Martin, E. and Willemet, J.-M.: The detailed snowpack scheme Crocus and its implementation in SURFEX v7.2. Geosci. Model Dev., Vol. 5, pp. 773–791, https://doi.org/10.5194/gmd-5-773-2012, 2012.

Vionnet, V., Marsh, C. B., Menounos, B., Gascoin, S., Wayand, N., Shea, J., Mukherjee, K. and Pomeroy, J.: Multi-scale snowdrift-permitting modelling of mountain snowpack. The Cryosphere, Vol. 15, pp. 743–769, https://doi.org/10.5194/tc-15-743-2021, 2021.

Vionnet, V., Verville, M., Fortin, V., Brugman, M., Abrahamowicz, M., Lemay, F., Thériault, M., Lafaysse, T. and Milbrandt, J.-A.: Snow level from post-processing of atmospheric model improves snowfall estimate and snowpack prediction in mountains. Water Resour. Res., Vol. 58, e2021WR031778, https://doi.org/10.1029/2021WR031778, 2022.

Viviroli, D., Dürr, H. H., Messerli, B., Meybeck, M. and Weingartner, R.: Mountains of the world, water towers for humanity: Typology, mapping, and global significance. Water Resour. Res., 43 (7), https://doi.org/10.1029/2006wr005653, 2007.

Viviroli, D., Kummu, M., Meybeck, M., Kallio, M. and Wada, Y.: Increasing dependence of lowland populations on mountain water resources. Nature Sustainability, Nature Publishing Group, 3(11), pp. 917–928, https://doi.org/10.1038/s41893-020-0559-9, 2020.

Warscher, M., Strasser, U., Kraller, G., Marke, T., Franz, H. and Kunstmann, H.: Performance of complex snow cover descriptions in a distributed hydrological model system: A case study for the high Alpine terrain of the Berchtesgaden Alps. Water Resour. Res., Vol. 49, pp. 2619–2637, https://doi.org/10.1002/wrcr.20219, 2013.

Warscher, M., Marke, T., Rottler, E. and Strasser, U.: Operational and experimental snow observation systems in the upper Rofental: data from 2017 to 2023. Earth Syst. Sci. Data Discuss. EGUsphere [preprint], https://doi.org/10.5194/essd-2024-45, 2024.

Weber, M.: A parameterization for the turbulent fluxes over melting surfaces derived from eddy correlation measurements. In: Strasser, U. and Vogel M. (eds.) (2008): Proceedings of the Alpine*Snow*Workshop, Munich, October 5–6, 2006, Germany. Berchtesgaden National Park research report 53, ISBN13 978-3-922325-60-4, Berchtesgaden, 2008.

Yokoyama, R., Shirasawa, M. and Pike, R. J.: Visualizing topography by openness: a new application of image processing to digital elevation models. Photogr. Eng. Rem. Sens., Vol. 68, pp. 257–266, 2002.